JOURNAL OF PETROLOGY | VOLUME 55 | NUMBER 8 | PAGES 1511–1533 | 2014 | doi:10.1093/petrology/egu032

Post-supereruption Magmatic Reconstruction of Taupo Volcano (New Zealand), as Reflected in Zircon Ages and Trace Elements

S. J. BARKER[1]*, C. J. N. WILSON[1], E. G. C. SMITH[1], B. L. A. CHARLIER[2], J. L. WOODEN[3], J. HIESS[1] AND T. R. IRELAND[4]

[1]SCHOOL OF GEOGRAPHY, ENVIRONMENT AND EARTH SCIENCES, VICTORIA UNIVERSITY OF WELLINGTON, PO BOX 600, WELLINGTON 6140, NEW ZEALAND

[2]DEPARTMENT OF PHYSICAL SCIENCES, CEPSAR, THE OPEN UNIVERSITY, WALTON HALL, MILTON KEYNES MK7 6AA, UK

[3]SUMAC, DEPARTMENT OF GEOLOGICAL AND ENVIRONMENTAL SCIENCES, STANFORD UNIVERSITY, STANFORD, CA 94305, USA

[4]RESEARCH SCHOOL OF EARTH SCIENCES, THE AUSTRALIAN NATIONAL UNIVERSITY, CANBERRA, ACT 0200, AUSTRALIA

RECEIVED NOVEMBER 14, 2013; ACCEPTED MAY 22, 2014

New zircon U–Th model-age and trace element datasets are presented from Taupo volcano (New Zealand), which are used to investigate the timescales and broad-scale magmatic processes involving zircon crystallization after the caldera-forming 25·4 ka Oruanui supereruption. Detailed ^{14}C-based chronologies and controls on vent locations allow the timing and location of post-caldera eruptions to be spatially and temporally constrained to an extent not possible for any other supervolcano. After ~5 kyr of post-Oruanui quiescence, Taupo erupted three dacitic units, followed by another ~5 kyr break, and then a sequence of rhyolitic units in three subgroups (SG1–SG3) from 12 ka onwards. Despite overlapping vent sites and crustal source domains between the Oruanui and post-Oruanui eruptions, U–Th zircon model ages in Taupo SG1 rhyolites (erupted from 12 to 10 ka) indicate only minor inheritance of crystals from the Oruanui magma source. Post-Oruanui model-age spectra are instead typically centred close to eruption ages with subordinate older pre-300 ka equiline grains in some units. U–Pb dating of these older grains shows that both 300–450 ka plutonic-derived and pre-100 Ma greywacke basement-derived zircons are present. The former largely coincide in age with zircons from the 350 ka Whakamaru eruption products, and are dominant over greywacke in young units that were vented within the outline of the Whakamaru caldera. Despite multiple ages and vent sites, trace element compositions are broadly similar in zircons, regardless of their ages. However, a small subset of zircons analysed from SG1 rhyolite (Units B and C) have notably high concentrations of U, Th, P, Y + (REE)$^{3+}$ and Nb but with only minor variations in Hf and Ti. SG2 zircons typically have higher Sc contents, reflecting large-scale changes in melt chemistry and crystallizing mineral phases with time. The age spectra indicate that most Oruanui zircons were removed by thermally induced dissolution immediately following the supereruption. U–Th ages from single post-Oruanui eruptions show consistent inheritance of post-Oruanui grains with model ages that centre between the temporally separated but geographically overlapping eruption groups, generating model-age modes. Within the statistical limitations of the isotopic measurements, we interpret these repeated modes to be significant, resulting from incorporation of crystal populations from cyclic post-Oruanui periods of magmatic cooling and crystallization, acting within a crustal protolith chemically independent of that which was dominant in the Oruanui system. These periods of cooling and crystallization alternate with times of rejuvenation and eruption, sometimes

* Corresponding author. Telephone: (+64) 4 463 9510. Fax: (+64) 4 463 5186. E-mail: smnbarker@gmail.com

demonstrably accompanying syn-eruptive regional rifting and mafic magma injection. Not only were the processes that developed the supersized Oruanui magma body rapid, but this huge magma system was effectively reset and rebuilt on a comparably short timescale.

KEY WORDS: *supereruption; Taupo Volcanic Zone; zircon; Taupo volcano; rhyolite*

INTRODUCTION

Large silicic magma systems play host to some of the most hazardous volcanoes on Earth, which are capable of erupting vast amounts of material in single events referred to as supereruptions, ejecting $\geq 10^{15}$ kg or ~ 450 km^3 of magma (Self, 2006). Numerous studies have addressed how silicic volcanic systems can accumulate large volumes of magma and release them in catastrophic caldera-forming events (e.g. Hildreth, 1981; Bachmann *et al.*, 2002; Vazquez & Reid, 2004; Wilson *et al.*, 2006; Reid, 2008; Saunders *et al.*, 2010; Allan *et al.*, 2012, 2013; Matthews *et al.*, 2012). Such studies typically focus on physical, geochemical and petrological investigations of the eruptive products, from either precursory leaks or the climactic eruption itself. However, less widely addressed is what happens to the host magma system [i.e. the melt-dominant zone, crystal mush zone and crustal reservoir of Hildreth & Wilson (2007)] immediately following a supereruption and how, and on what timescales, the volcano moves into subsequent activity. Does the supereruption act to reset the host magma system and the volcano's eruptive behaviour, or does it merely represent another, exceptionally large eruption from a long-lived magma system?

A method that has proved invaluable in the interpretation of magmatic processes in large silicic magma systems is single-crystal dating of zircon ($ZrSiO_4$) by U–Pb or U–Th disequilibrium techniques. Zircon model-age data can provide insights into the timing and rates of magma accumulation (Brown & Fletcher, 1999; Reid & Coath, 2000; Vazquez & Reid, 2002; Simon & Reid, 2005; Wilson & Charlier, 2009; Schmitt *et al.*, 2010; Storm *et al.*, 2011), the range of magmatic and crustal sources that contribute melt and crystals to the system (Reid *et al.*, 1997; Bindeman *et al.*, 2001; Charlier *et al.*, 2010), and the temporal evolution of the magma system as a whole (Simon *et al.*, 2009; Watts *et al.*, 2012). Zircon trace element compositions can also be used with age data to infer changes in melt composition and modal assemblage (e.g. Barth *et al.*, 2013). However, supereruptions are inferred to occur globally only once every $\sim 10^5$ years (Mason *et al.*, 2004; Miller & Wark, 2008). Their relative scarcity in the geological record controls interpretations of the post-supereruption magmatic temporal record through the uncertainties of the geochronological techniques used. For example, fine detail of eruptive events and magmatic processes is constrained by the 10^4–10^5 year uncertainties using $^{40}Ar/^{39}Ar$ and U–Pb systematics (e.g. Simon *et al.*, 2008), making the study of closely spaced post-caldera magmatism difficult. In addition, there is a range of post-supereruption behaviour, varying from rapid (thousands to tens of thousands of years) magmatic and structural resurgence of less evolved magmatic dregs (e.g. Valles: Stix *et al.*, 1988; Phillips *et al.*, 2007; Toba: Chesner, 2012; La Pacana: Lindsay *et al.*, 2001; Long Valley: McConnell *et al.*, 1995; Hildreth, 2004) or rapid construction of a post-caldera composite cone (e.g. Aira: Aramaki, 1984), to longer-term (hundreds of thousands of years) systematic tapping of magma incorporating recycled hydrothermally altered crystal mush or caldera infill (e.g. Yellowstone caldera: Bindeman *et al.*, 2001; Girard & Stix, 2009; Vazquez *et al.*, 2009).

Here we investigate a case study of post-supereruption recovery at Taupo volcano, (Fig. 1; Wilson *et al.*, 1995), using ^{238}U–^{230}Th disequilibrium and ^{238}U–^{206}Pb dating techniques, coupled with trace element analyses of zircons. Taupo is source to the 530 km^3 (magma) Oruanui eruption at $\sim 25{\cdot}4 \pm 0{\cdot}2$ ka, which is the world's youngest example of a supereruption (Wilson, 2001; Wilson *et al.*, 2006; Vandergoes *et al.*, 2013). Taupo in particular provides a unique circumstance to investigate the development and post-caldera recovery of a large silicic magmatic system for several reasons. First, the frequency of eruptions is exceptionally rapid. Only ~ 5 kyr after the Oruanui eruption, Taupo resumed activity with a total of 28 eruptions to the present day (Wilson, 1993), providing frequent snapshots of the magmatic system. Second, the young age and good preservation of Taupo's eruptive products provides a high-resolution age record. Eruption timings are radiocarbon dated with 1SD (standard deviation) uncertainties of 10^2–10^3 years, and magmatic chronologies can be interrogated by U–Th disequilibrium techniques on zircon with 10^3–10^4 year 1SD uncertainties (Charlier *et al.*, 2005; Wilson & Charlier, 2009). Third, existing field, geochemical and petrological data provide many constraints on the broad evolution of both the pre- and post-supereruption magmatic systems (e.g. Sutton *et al.*, 1995, 2000; Wilson *et al.*, 2006) and for the young products of the nearby NE dome magmatic system (Fig. 1; Sutton *et al.*, 1995; Wilson & Charlier, 2009). In this study we present new zircon model-age data and trace element data for eight post-Oruanui eruptions and compare and contrast them with new trace element data for Oruanui zircons, and pre-existing zircon age spectra for both the Oruanui and pre-Oruanui products (Charlier *et al.*, 2005; Wilson & Charlier, 2009). By comparing these data we demonstrate how Taupo's young magmatic system was destroyed and then rebuilt on rapid timescales (thousands of years), into a system that appears to have little or no direct relationship to that which previously fed a supereruption.

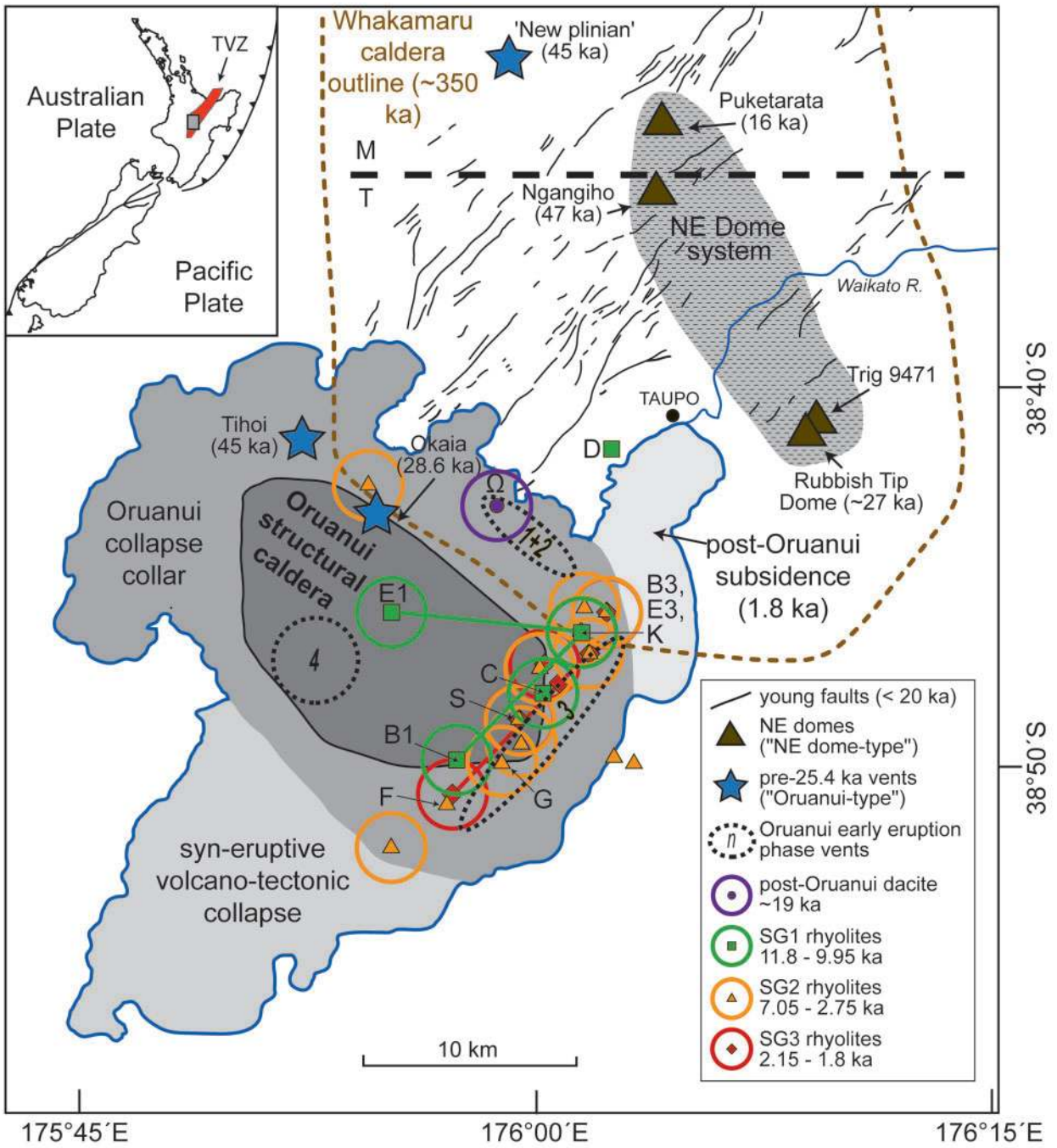

Fig. 1. Regional setting and structural features of Taupo volcano in the Taupo Volcanic Zone (TVZ), New Zealand (map inset) [modified from Wilson & Charlier (2009)]. Lineations are young NNE–SSW surface faults. Areas defined under Lake Taupo are the structural elements of the Oruanui caldera and subsequent collapse events after Wilson (2001). The bold horizontal black dashed line marks the arbitrary boundary between the Taupo (T) and Maroa (M) volcanoes, and the fine dashed line represents the inferred Whakamaru caldera boundary (Wilson *et al.*, 1986). Pre-Oruanui vent sites, ages and magma types are after Wilson & Charlier (2009), and approximate vent areas for the first four phases of the Oruanui eruption are from Wilson (2001). Inferred vent sites and ages for the post-Oruanui eruption groups are modified from Wilson (1993), with labelled units representing eruptions investigated in this study and tie-lines representing shifting vents within single eruptions. The shift of vent site between the Ω dacite and rhyolites, and the cluster of vent sites near the eastern shore, especially for the recent eruptions, should be noted.

GEOLOGICAL BACKGROUND

Taupo volcano is located in the southern part of the central Taupo Volcanic Zone (TVZ), in the North Island of New Zealand (Fig. 1; Wilson *et al.*, 1995, 2009). Taupo volcano and its northern neighbour Maroa are superimposed on a large caldera associated with the 350 ka Whakamaru group of ignimbrites (Fig. 1; Wilson *et al.*, 1986; Leonard *et al.*, 2010). Taupo has been active in close relation with Maroa since ~300 ka, but its early history is poorly known because of limited age data and burial by younger deposits (Leonard, 2003; Wilson *et al.*, 2009). From ~65 ka, explosive activity became more focused towards vents now concealed by Lake Taupo, and minor activity from Maroa became almost exclusively accompanied by lava extrusion. Between ~65 ka and the Oruanui eruption (25·4 ka), there were ~11 eruptions from the Taupo–Maroa area, with five of these linked to two distinctive magma types (Sutton *et al.*, 1995; Wilson & Charlier, 2009; Fig. 1). The 'Oruanui-type' magma (Wilson *et al.*, 2006) was of broadly similar composition and mineralogy to the Oruanui rhyolite and is considered to represent precursor leaks of that magma system (Fig. 2). The 'NE-dome-type' magma (Sutton *et al.*, 1995), had a higher crystal content, biotite as an additional crystal phase and contrasting $^{87}Sr/^{86}Sr$ to the Oruanui-type magmas (Fig. 2; Wilson & Charlier, 2009). It was erupted from a series of vents to the NE of modern Lake Taupo, overlapping with Maroa lava domes (Fig. 1).

The Oruanui event evacuated >530 km^3 of magma; >99% rhyolitic and <1% mafic, over 10 phases during a prolonged, episodic phreatomagmatic eruption (Wilson, 2001; Wilson *et al.*, 2006; Van Eaton & Wilson, 2013). Contrasts in U–Th model-age spectra between zircons from the precursor Oruanui-type magmas and the Oruanui magma itself (Wilson & Charlier, 2009) and element diffusion modelling (Allan *et al.*, 2013) indicate that the 530 km^3 melt-dominant body was accumulated in at most about 3000 years. Assembly of the Oruanui magma body was not only rapid, but included contributions from Quaternary intrusions and melts from greywacke metasediments that were introduced into the magma body up to the point of eruption (Liu *et al.*, 2006; Charlier *et al.*, 2008). Oruanui pumices show evidence for mixing in both bulk-rock compositions and mineral populations, implying that any systematic zonation in the system was disrupted by vigorous convection prior to eruption (Wilson *et al.*, 2006). In addition, during the first two eruption phases, there was lateral movement of 'NE-dome-type' magma into the Oruanui vent controlled by syn-eruptive rifting (Allan *et al.*, 2012).

Following the Oruanui eruption, the behaviour of Taupo changed markedly. Temporally separated clusters of eruptions occurred from vent sites that geographically overlapped (Fig. 1; Wilson, 1993), with chemical compositions that are distinct from those of Oruanui or pre-Oruanui magmas (Fig. 2; Sutton *et al.*, 2000; Wilson & Charlier,

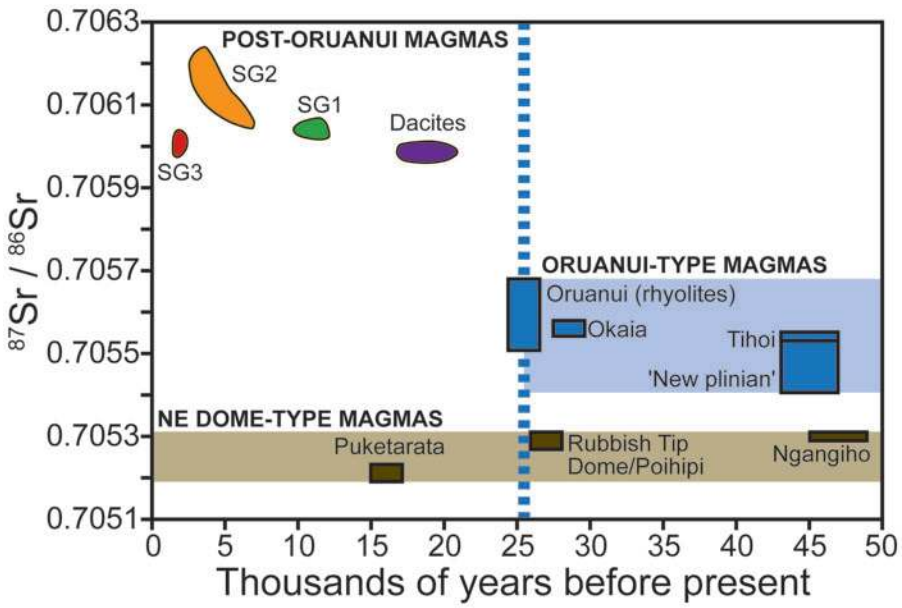

Fig. 2. $^{87}Sr/^{86}Sr$ variations in magmas erupted from the Taupo–Maroa region over the last 50 kyr. Noteworthy features are the two contrasting Oruanui-type and NE dome-type magmas erupted prior to the Oruanui supereruption, and the apparent continuity of the NE dome system, but large compositional shift in the post-Oruanui magmas despite overlapping vent sites (Fig. 1). Inferred ages and compositions for the NE dome-type and Oruanui-type magmas are from Sutton *et al.* (1995), Charlier *et al.* (2005), Wilson *et al.* (2006) and Wilson & Charlier (2009). The new 25·4 ka eruption age for the Oruanui is from Vandergoes *et al.* (2013). Post-Oruanui eruption ages are from Wilson (1993), and isotopic compositions are from Sutton *et al.* (2000).

2009). The first three eruptions from 20·5 to 17 ka were dacitic (Units Ψ, Ω and A), with vent sites in the northern sector of the Oruanui caldera. The remaining 25 eruptions fall into three chemically distinct rhyolitic subgroups, erupted from multiple vent sites within and beyond the caldera margin in discrete periods from ~11·8 to 9·95 ka (Subgroup 1, Units B to E), 7·05 to 2·75 ka (Subgroup 2, Units F to W) and 2·15 to 1·8 ka (Subgroup 3, Units X to Z: Wilson, 1993; Sutton *et al.*, 2000).

In the post-Oruanui sequence we focus on eight eruptions of the Subgroup 1 (SG1) rhyolites (Units B, C, D and E) and Subgroup 2 (SG2) rhyolites (Units F, G, K and S) to investigate the post-caldera magmatic reconstruction of Taupo. For two of these eruptions (B and E), we have analysed zircons from two subunits for each respective eruption (B1 and B3; E1 and E3) which represent products from different vents during the eruptions (Fig. 1; Wilson, 1993). Previous work on the dacitic Unit Ω showed that its zircons are mostly inherited grains from older plutonic and country rock melts (Charlier *et al.*, 2010), and we have carried out reconnaissance U–Pb determinations of Units D and F where equiline grains dominate the zircon population analysed. We have not analysed zircons from the third subgroup of rhyolites owing to their relative scarcity (Charlier *et al.*, 2005).

ANALYTICAL TECHNIQUES

Samples used for zircon separation consisted of multiple pumices (Units B, C, E, G, K and S) or blocks of pumiceous dome carapace (Units D and F) (see Supplementary Data: Electronic Appendix A for sample details; all supplementary data are available for downloading at http://www.petrology.oxfordjournals.org). Each sample was cleaned and crushed, then sieved to 250–125 μm, 125–63 μm and <63 μm. Zircons were separated using conventional heavy liquid and magnetic separation methods similar to those of Charlier *et al.* (2005), with the additional use of a Wilfley gravity table to obtain an initial heavy mineral concentrate from bulk crushed material. The majority of zircons obtained in this study were in the 63–125 μm size fraction, with very few zircons recovered that were larger than 125 μm. Zircons were mounted in epoxy resin, polished to expose the cores of the grains and imaged by cathodoluminescence (CL). Representative CL images of zircon textures with corresponding age and trace element spots are presented in Supplementary Data: Electronic Appendix B.

U–Th zircon analyses were carried out by secondary ion mass spectrometry (SIMS) using the USGS-Stanford SHRIMP-RG (sensitive high-resolution ion microprobe with reverse geometry) with techniques modified from those of Charlier & Wilson (2010). Prior to data acquisition, a 50 μm × 50 μm square region was rastered for 2 min to remove the Au surface coating and any contamination. Ions were then sputtered from zircons with a 14–17 nA $^{16}O_2^-$ primary ion beam focused to a 35–40 μm spot. Data were collected in six scans per point for $^{90}Zr_2{}^{16}O$, $^{180}Hf^{16}O$, ^{206}Pb, ^{207}Pb, ^{208}Pb, $^{230}Th^{16}O$, $^{232}Th^{16}O$, $^{235}U^{16}O$ and $^{238}U^{16}O$. Dwell times ranged from 2 to 40 s for each peak. To allow for the low U contents of the zircons $^{230}Th^{16}O$ and the background (at mass 246·16 u) were measured for 60 s on each scan. Analyses that produced low $^{230}Th^{16}O$ counts within 3SD uncertainty of the background were discarded (<5 analyses in total). Additionally, a measurement at mass 244 (corresponding to $^{232}Th^{12}C^+$) for 10 s was used to check for the beam impinging on the epoxy and, if significantly higher than background, the measurement was discarded (<10 analyses in total). A U–Th fractionation factor was empirically determined by repeated analyses of multiple zircon standards run on the same mounts as the unknowns. The standards included MAD (Madagascar green: Barth & Wooden, 2010) as the concentration standard, R33 (Black *et al.*, 2004), VP10 (1200 Ma, granitoid, Joshua Tree National Park, CA; A. P. Barth & J. L. Wooden, unpublished data) and zircons from the earliest Bishop Tuff fall deposit (Chamberlain *et al.*, 2014). Given their ages, ^{238}U and ^{230}Th activities in these zircon standards are at secular equilibrium and after the application of a U–Th fractionation factor, the calculated ($^{230}Th/^{238}U$) should equal unity, determined on a mount-by-mount basis using the measured $^{238}U^{16}O^+/^{230}Th^{16}O^+$ ratios. Calculated fractionation factors from each analytical session were used to correct the ($^{238}U/^{232}Th$) of the unknowns, and repeated analysis of the standards over the sessions allowed us to derive a best-estimate 1σ error of ± 1·2% on the fractionation factor (see Charlier *et al.*, 2005).

Values of the ($^{238}U/^{232}Th$) and ($^{230}Th/^{232}Th$) ratios (values in parentheses denote activity ratios) for whole-rock (WR) samples for Units B1, D, E3, G and S were previously determined by isotope-dilution thermal ionization mass spectrometry (ID-TIMS) and reported by Charlier *et al.* (2005). For Units B3, C, E1, F and K, the ($^{230}Th/^{232}Th$) was determined on unspiked dissolutions by multi-collector inductively coupled plasma mass spectrometry (MC-ICP-MS) using a Thermo-Finnigan Neptune instrument at the Open University, and ($^{238}U/^{232}Th$) was calculated from U and Th concentration analyses determined using a Thermo Scientific Element2 sector-field ICP-MS system at Victoria University of Wellington. Previous comparisons of the two techniques used have shown that they produce identical data within analytical uncertainty (Wilson & Charlier, 2009). ^{230}Th–^{238}U isochron ages were calculated as two-point model ages by referencing each of the fractionation-corrected zircon analyses to the respective whole-rock analysis on the equiline diagram (see Supplementary Data: Electronic Appendix C for raw U–Th model-age data).

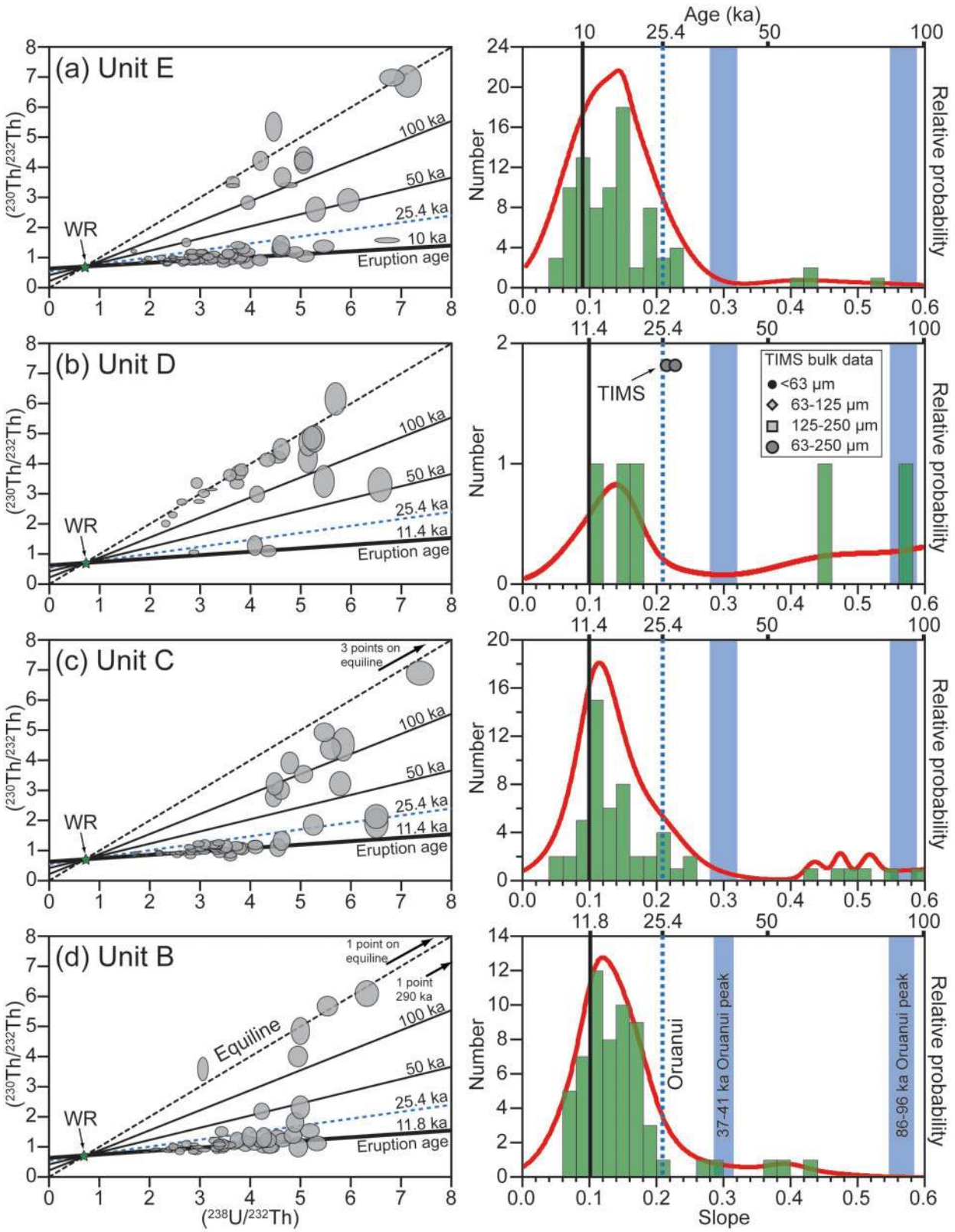

Fig. 3. Zircon equiline diagrams and corresponding histograms for SG1 eruptions: (a) Unit E (10 ka); (b) Unit D (11·4 ka); (c) Unit C (11·4 ka); (d) Unit B (11·8 ka). Reference isochrons on (^{230}Th/^{232}Th) vs (^{238}U/^{232}Th) equiline diagrams indicate the eruption age estimates

(continued)

U–Pb zircon age determinations were carried out using the SHRIMP-RG instrument at the Research School of Earth Sciences, Australian National University (ANU). To minimize contamination by common Pb, the mounts were cleaned in detergent, petroleum spirits, alcohol and 1N HCl with intervening rinses in distilled water. The primary beam was rastered over an area of 35 μm × 45 μm prior to data acquisition to remove the gold coating and any surface contamination. Secondary ions were sputtered from zircons with a 5–6 nA primary O_2^- beam focused to a 25 μm × 35 μm spot. Two suites of data were collected. The first was applied to zircons from samples of eruption D and E. The mass spectrometer was cycled in six scans per spot through peaks corresponding to $^{90}Zr_2{}^{16}O$, ^{204}Pb, background, ^{206}Pb, ^{207}Pb, ^{208}Pb, ^{238}U, $^{232}Th^{16}O$ and $^{238}U^{16}O$. Because of the young ages of the grains and hence the low count rate, ^{206}Pb and ^{207}Pb were counted for 30 and 20 s respectively. The second suite of data was collected from zircons from the lava dome of eruption F. In this case, because we wanted to fingerprint the grains simply into three broad categories (greywacke; Quaternary with resolvable ^{206}Pb counts; ^{206}Pb not distinguishable from background) the same magnet cycle was used, but with only a single scan through the mass table. In all cases, SL-13 was used as a concentration standard (238 ppm U) and R33 was used as an age standard (420 Ma) (Black *et al.*, 2004). To account for initial ^{230}Th disequilibrium in the ^{238}U–^{206}Pb decay chain, a Th/U correction factor was applied using $f = (Th/U_{zir})/(Th/U_{magma})$ (Schärer, 1984) based on the observed Th and U concentrations of the zircons derived from SIMS measurements and whole-rock Th/U values measured as previously described. A correction for common Pb was applied using the recorded $^{207}Pb/^{206}Pb$ values and a common Pb isotopic composition ($^{207}Pb/^{206}Pb = 0{\cdot}836$) for the sample age from the average crust model of Stacey & Kramers (1975). (See Supplementary Data: Electronic Appendix D for further details and all sample data for U–Pb analyses.)

Zircon trace element analyses were carried out after age dating by SIMS using the SHRIMP-RG at Stanford University with a 1·5–3 nA primary beam and a focused 15 μm × 12 μm spot. Trace element analytical spots were not made directly on the U–Pb or U–Th age dating spots, but instead the opposite growth zone to that dated was analysed or the mounts were repolished to remove the age pits prior to analysis (Supplementary Data: Electronic Appendix B). Analysis spots were also selected to avoid contamination by inclusions or crystal defects visible in reflected light images. We used common elements that are normally found at very low concentrations in zircon to monitor such contamination: Ca, Al, Na and K for feldspar and glass; Ca, P and F for apatite; Fe for Fe–Ti oxides; and Ca and Fe for allanite. The MAD zircon standard (Barth & Wooden, 2010) was used to calibrate trace element concentrations (see Supplementary Data: Electronic Appendix E for trace element data and standards data).

RESULTS

U–Th model ages

Zircon U–Th model ages for the SG1 rhyolites show two patterns (Fig. 3), which reflect contrasts in vent location and style of eruption (Fig. 1). For the pyroclastic Units B, C and E, vented from within the modern Lake Taupo, age spectra are dominated by young zircons with the majority being close to eruption ages (~10–12 ka, or slope 0·10). A subordinate number of analyses form either a tail-off to slightly older ages with secondary minor (or major for Unit E) peaks between slopes 0·14 and 0·20 (Fig. 3a, c and d). Less than 5% of the zircons in these units gave equiline values corresponding to ages >300 ka. For the eruptions that had a shift in vent (subunits B1–B3 and E1–E3), there are only minor differences between the subunit age spectra, with all showing similar bimodal or skewed age populations in histograms (Fig. 4). In contrast, Unit D, which is of much smaller volume and was erupted outside the structural caldera and modern lake (Fig. 1), has a zircon population that is dominated by older grains that lie on or within 1 SD uncertainty of the equiline (Fig. 3b). Only three of 25 zircons analysed from this sample (12%) gave young post-Oruanui ages, averaging ~16 ka. Notably, in our new work we recorded very few zircons with model ages matching the dominant Oruanui zircon U–Th age peaks at ~34–41 ka and 86–95 ka [Figs 3 and 4: Wilson & Charlier (2009)]. These data contrast somewhat with those presented by Charlier *et al.* (2005), and the reasons for this are considered below.

Similar trends in U–Th model-age spectra are observed in the SG2 rhyolites, which are dominated by post-Oruanui zircons (Fig. 5). Although these samples generally had lower zircon yields (e.g. Charlier *et al.*, 2005), they

Fig. 3. Continued
from Wilson (1993) and 50 and 100 ka. Error ellipses represent 1SD analytical uncertainties on ($^{230}Th/^{232}Th$) and a standard 3% error on ($^{238}U/^{232}Th$) [see Charlier *et al.* (2005) for further details]. An isochron slope and age was determined by referencing these isotopic data points to the whole-rock (WR) values to generate a two-point model age (see text for details). Probability density function (PDF) curves (from Isoplot; Ludwig, 2008) and histograms are based on isochron slopes derived from two-point whole-rock zircon SIMS determinations. The PDF line is based on the two-point isochron slopes, rather than the ages determined from them, as the uncertainties are symmetrical with respect to the slope value. Multi-zircon TIMS data points are from Charlier *et al.* (2005). The two reference Oruanui peaks are taken from Wilson & Charlier (2009). Analytical data and model ages are given in Supplementary Data: Electronic Appendix C. TIMS legend shows size fractions denoted in Figs 3, 4 and 5.

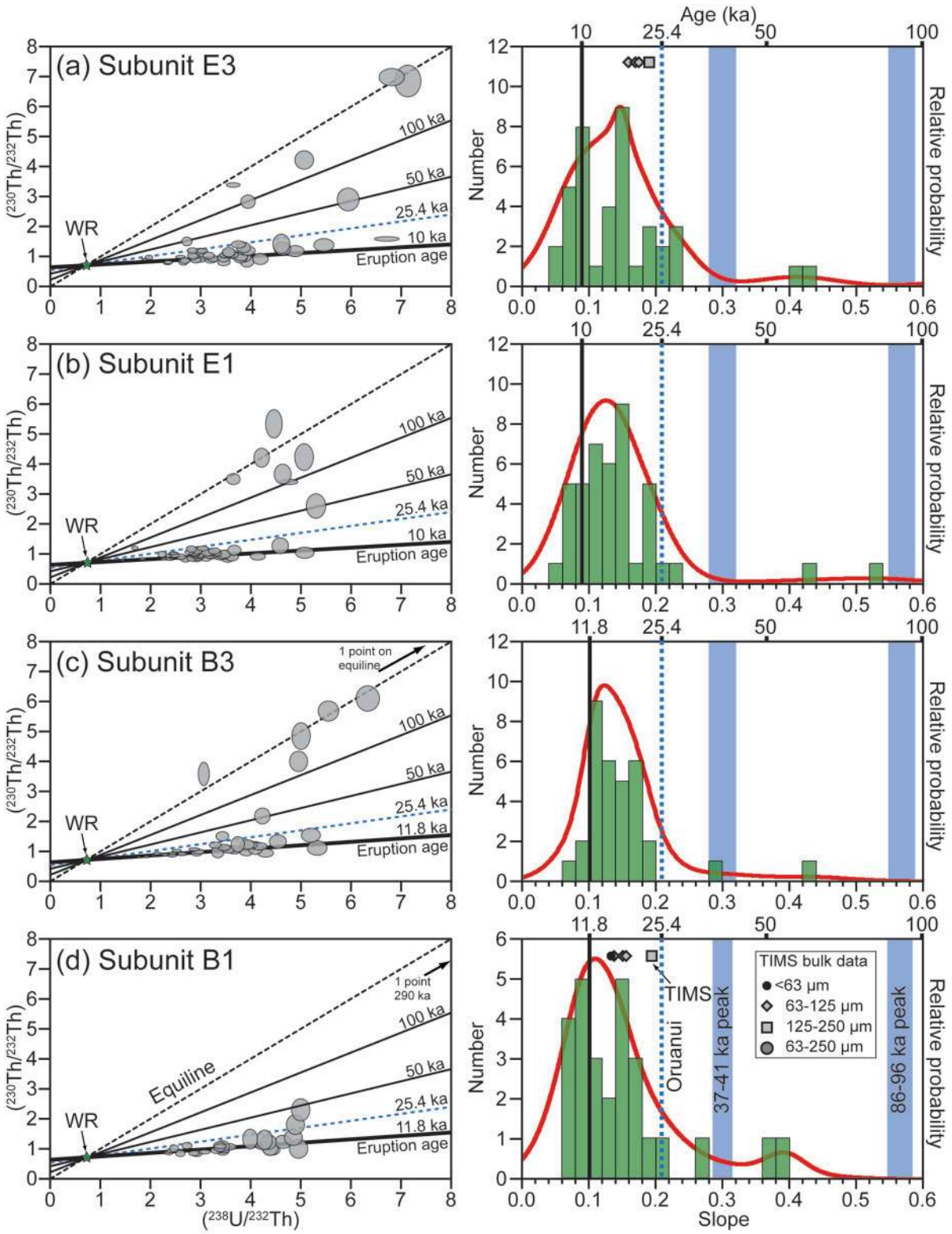

Fig. 4. Zircon equiline diagrams and corresponding histograms for SG1 eruption subunits where there were co-eruptive shifts in vent position. (a) Subunit E3, vented from the eastern part of Taupo caldera. (b) Subunit E1 from the western–central caldera. (c) Subunit B3 from the eastern part of the caldera. (d) Subunit B1 from the southeastern segment of the caldera. Details as in Fig. 3. Eruption vent sites are shown in Fig. 1 (from Wilson, 1993). TIMS data are from Charlier *et al.* (2005). Analytical data and model ages are given in Supplementary Data: Electronic Appendix C.

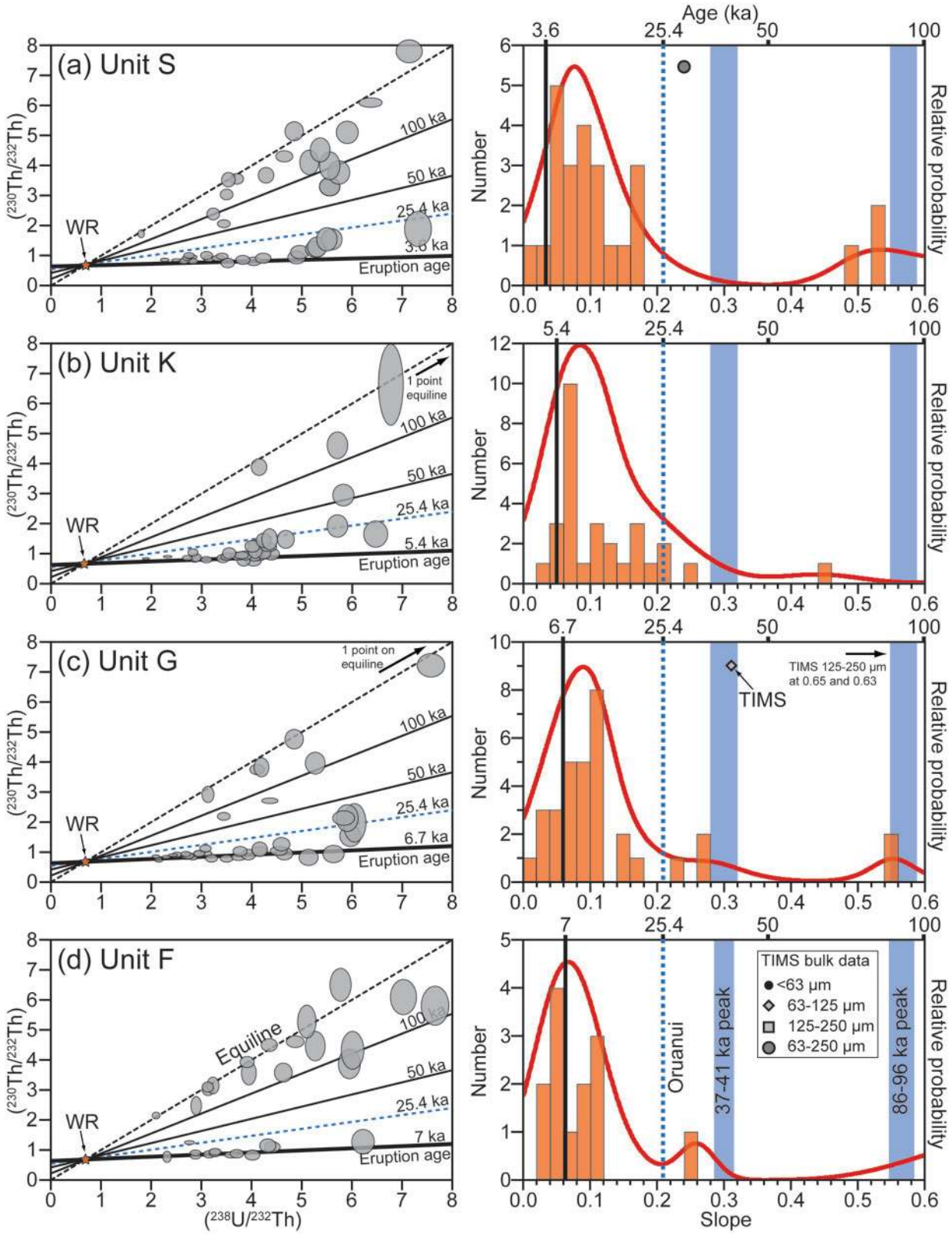

Fig. 5. Zircon equiline diagrams and corresponding histograms for SG2 eruptions: (a) Unit S (3·6 ka); (b) Unit K (5·4 ka); (c) Unit G (6·7 ka); (d) Unit F (Motutaiko Island) (7 ka). Details as in Fig. 3. Eruption vent sites are shown in Fig. 1, from Wilson (1993). TIMS data are from Charlier *et al.* (2005). Analytical data and model ages are given in Supplementary Data: Electronic Appendix C.

still contain phenocrystic zircons with ages within analytical uncertainty of their eruption ages. In addition, the SG2 samples also show two slightly older age populations. The first is present to some extent in all the eruption products sampled (being the dominant peak in Unit G) and overlaps with the eruption ages of the SG1 rhyolites. Despite the magnitude of the analytical uncertainties involved with single U–Th model ages (see Discussion section), this age peak is notably consistent between all the eruptions studied. A less well-defined subordinate peak or upper tail, similar in position to the secondary peak observed in the SG1 rhyolites, is also present in Units G, K and S (Fig. 5a–c). Unit F differs slightly from the other SG2 units as it contains a mixed proportion of 'young' and 'old' (equiline, >300 ka) zircons, and no minor peak (Fig. 5d). In similar fashion to Unit D from SG1, Unit F was of smaller volume than the other SG2 rhyolites studied, and was erupted from the most peripheral (southerly) vent site for eruptions considered in this study (Fig. 1).

U–Pb ages

Zircons that gave U–Th ages within 1SD uncertainty of the equiline and some grains that appeared to have distinguishable cores of contrasting texture in CL imaging were selected for further analysis by U–Pb methods (see Supplementary Data: Electronic Appendix B for CL images). In particular, zircons from Units D and F were studied owing to their contrasting U–Th model-age spectra from the other samples and their abundance of equiline grains (Figs 3b and 5d; Supplementary Data: Electronic Appendix C). In addition, a few zircon cores from Unit E1 were analysed for comparison, but only a single grain gave an age of >300 ka. For Unit D (Acacia Bay Dome), the majority of equiline zircons and distinguishable cores produced U–Pb ages of <500 ka, with only one of 30 grains analysed giving an older age of ~2·5 Ma. Interestingly, the U–Pb zircon age spectrum of the Unit D sample, which lies within the Whakamaru Caldera, closely aligns with that of the 350 ka Whakamaru eruption (Fig. 6; Brown & Fletcher, 1999; Matthews, 2011). In contrast, equiline zircons from Unit F (Motutaiko Island) towards the more southerly end of Lake Taupo are predominantly pre-100 Ma in age, with only a few grains (five of 23 analyses) identified as Quaternary in age (Supplementary Data: Electronic Appendix D).

Trace element compositions

Trace element compositions were determined on the same zircon grains (and growth zone where possible) as those analysed for U–Th or U–Pb dating. In addition to the post-Oruanui units, zircons from Oruanui phase 1 fall deposits with previous age determinations (sample P1634; Wilson & Charlier, 2009) were analysed for comparison. Overall, the majority of zircons analysed from the Oruanui and post-Oruanui zircons broadly overlap in trace element compositions, with similar U, Th, Hf, Ti, Y, rare earth elements (REE) and P concentrations (Fig. 7; Supplementary Data: Electronic Appendix E). However, a small subset of zircons (mainly core and interior analyses; Supplementary Data: Electronic Appendix B) from the SG1 rhyolite and Oruanui have significantly higher concentrations of U, Th, P, Y + $(REE)^{3+}$ and Nb but with only minor differences in Hf and Ti concentrations. When zircons are ordered by model age, the SG1 zircons with high concentrations in U, Th, P, Y, $(REE)^{3+}$ and Nb, appear to be mainly from core zones with ages between 10 and 20 ka (Fig. 7). Sc and to a lesser extent Ti and P concentrations, in contrast, vary with relative ages across the whole zircon population, each showing an overall increasing trend in concentration with decreasing age. Some trace element ratios also show temporal changes. For example, Yb/Gd decreases with younger age and is consistently lower in zircons with post-Oruanui model ages. Th/U ratios show more scattered variations, but with a small proportion of post-Oruanui zircons (especially around ~10–20 ka model ages) displaying increased values. Notably, the few grains determined to be of

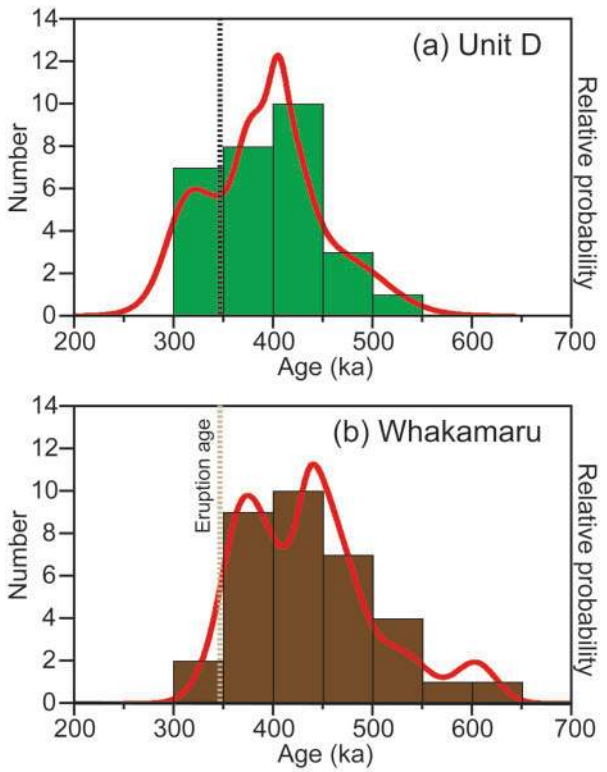

Fig. 6. Comparison of U–Pb age histograms (and population density curves) for xenocrystic zircons from (a) Unit D (Acacia Bay Dome), and (b) the Whakamaru ignimbrite reported by Brown & Fletcher (1999). (See text for discussion and Supplementary Data: Electronic Appendix D for raw data and ages.)

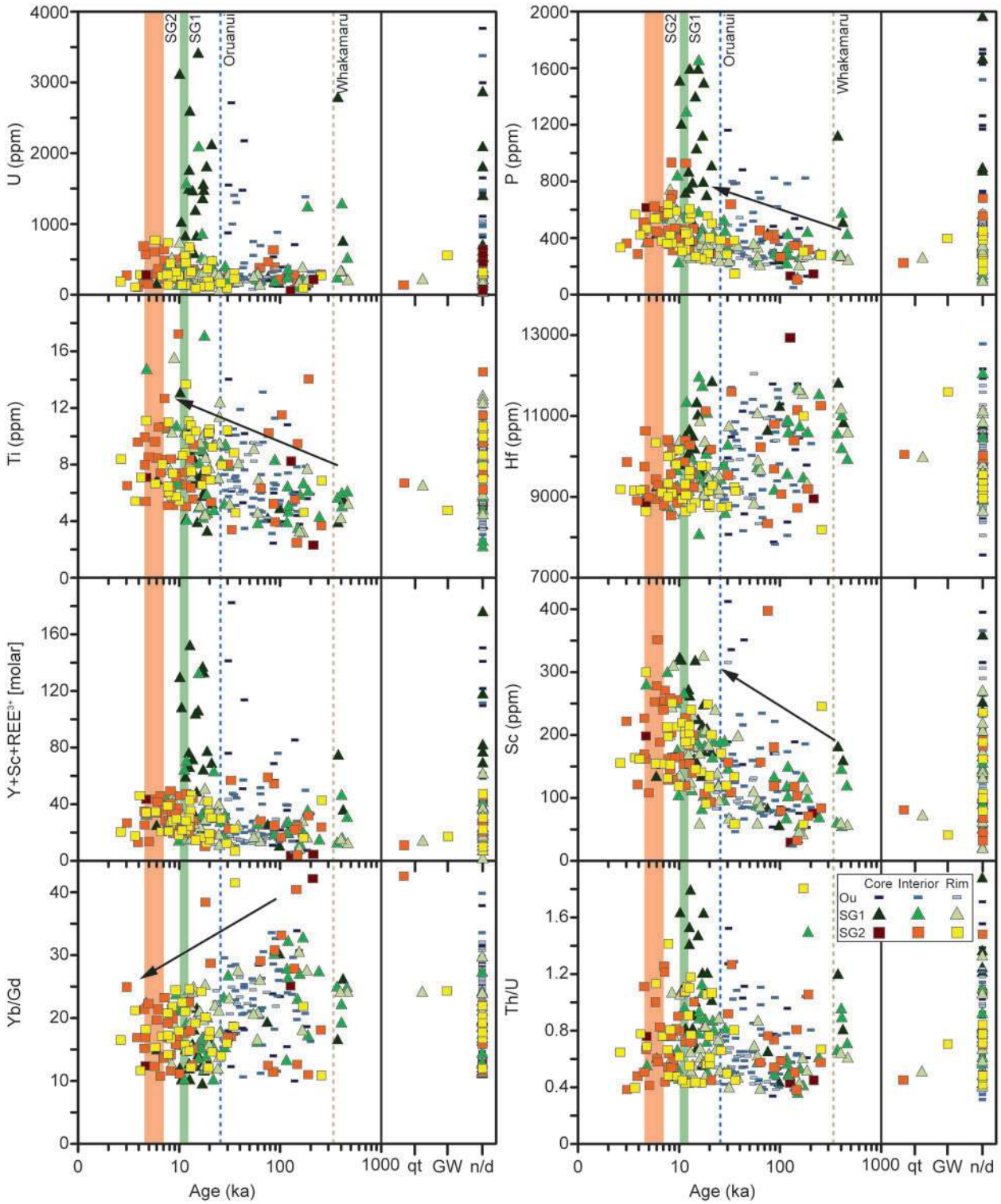

Fig. 7. Trace element abundances and ratios versus U–Th model ages for zircons from the Oruanui (Ou) and post-Oruanui eruptive rocks. For grains older than 1 Ma: qt, Quaternary; GW, greywacke (>l00 Ma); n/d, not determined. The relative ages of the Whakamaru and Oruanui eruptions are shown for reference. Arrows indicate direction of change with relative age. (See text for discussion.) Core analysis locations refer to analyses where clear cores could be identified. Interior zones are areas between the core or middle of the crystal and the outer edge or rim area. Representative CL images of zircon textures with corresponding age and trace element spots are given in Supplementary Data: Electronic Appendix B. All raw trace element data and details are given in Supplementary Data: Electronic Appendix E.

Whakamaru age, or other Quaternary, or pre-100 Ma ages are largely indistinguishable from younger grains on the basis of their trace element compositions alone (Fig. 7).

DISCUSSION

The zircon U–Th model-age spectra presented in this study provide unique insights into Taupo's young magmatic system, highlighting not only its evolution over very short timescales, but also the timing and nature of its post-supereruption recovery. One outstanding feature of the post-Oruanui U–Th model-age spectra, observed in all the units sampled, is the scarcity of zircons with ages matching the distinctive Oruanui spectrum, despite the relatively short period of quiescence and the significantly contrasting eruptive masses between the voluminous Oruanui and the more modestly sized post-Oruanui events. Previous work on Taupo has highlighted how the Oruanui melt-dominant body was formed over exceptionally short timescales (e.g. millennia to centuries: Wilson & Charlier, 2009; Allan *et al.*, 2013). Below we consider how that large magma system was effectively destroyed over comparably short timescales, and how the volcano adjusted, rebuilt and has maintained its new magma system.

Relationship between the pre- and post-Oruanui magma systems

The presence of the two distinctive magma systems operating in the Taupo–Maroa area in the lead-up to and during the Oruanui eruption has been documented from several perspectives (Sutton *et al.*, 1995; Charlier *et al.*, 2005; Wilson & Charlier, 2009; Allan *et al.*, 2012). Zircons from three precursor eruptions of Oruanui-type magmas have age spectra with a prominent peak at ~95 ka, indicating that they were sourced from a common mush zone (Wilson & Charlier, 2009). Zircon age spectra from Oruanui eruption samples share this 95 ka peak, but have an additional major peak at ~40 ka (Fig. 8). The contrast between the age spectra of the Oruanui and the youngest precursory Oruanui-type eruption (Okaia) at ~28·6 ka was used to infer that despite common roots, the two magma bodies were generated independently, with the Oruanui forming over <3000 years (Wilson & Charlier, 2009; Allan *et al.*, 2013).

The distinctive model-age spectra in the pre-Oruanui eruptive rocks mean that any recycled crystals from the old system should, in principle, be identifiable through their age spectra in the post-Oruanui deposits. In contrast, we record few zircons either of Oruanui age (~25·4 ka: <12% of the zircon population within 1SD, Fig. 8), or of age ranges coinciding with the 40 ka (<2% of zircons) or 95 ka (<5% of zircons) model-age modes in the Oruanui. Our new data contrast with the SIMS data previously

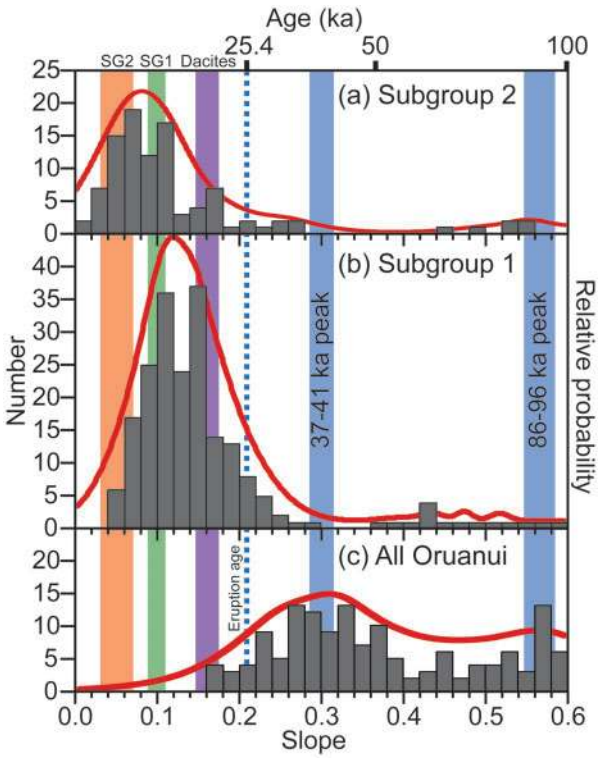

Fig. 8. Comparison of summary U–Th age histograms (and PDF curves) for (a) all SG1 rhyolites (Units B + C + D + E), (b) SG2 rhyolites (Units F + G + K + S) and (c) all Oruanui samples (early + late phases) from Wilson & Charlier (2009). The scarcity of Oruanui age or Oruanui peak-age grains in the SG1 and SG2 rhyolites, and the multiple young age modes, should be noted. [See Supplementary Data: Electronic Appendix C for all raw data and Wilson & Charlier (2009) for details on the Oruanui datasets.]

presented by Charlier *et al.* (2005) in that there is a much greater proportion of post-Oruanui model ages obtained from zircons in both Unit B samples, more in keeping with the multi-grain TIMS ages reported by Charlier *et al.* (2005). The most likely reason for this is a sampling bias, where larger grains containing zones with higher U and Th concentrations (typically cores: Supplementary Data: Electronic Appendix B) were specifically targeted by Charlier *et al.* (2005). In contrast, we have analysed a mixture of zircon rims, representing the youngest crystallization of zircon, and cores where discernible, representing older crystallization or possibly inherited grains (Supplementary Data: Electronic Appendix B and C). We consider this a less biased approach that more fully encompasses a representative range of zircon ages within the post-Oruanui rhyolites.

The scarcity of Oruanui eruption-age or peak-age (40 ka or 95 ka) zircons indicates that there was a significant change in Taupo's magmatic system following the Oruanui eruption. The paucity of Oruanui or pre-Oruanui modal age zircons in the younger eruptive rocks could reflect

several possible circumstances (or a combination thereof), as follows.

(1) The young magmas were sourced from a different crustal volume from that of the Oruanui and pre-Oruanui magmas. We consider this to be highly unlikely given the extensive implied volume of the Oruanui magma system and the geographically overlapping vent sites between the Oruanui and post-Oruanui eruptions (Fig. 1). For example, the likely vent location for Unit Ω overlaps with the inferred vent site for phases 1 and 2 of the Oruanui and the majority of the post-Oruanui rhyolite vents largely overlap with that of phase 3 (Fig. 1; Wilson, 1993, 2001). In addition, even eruptions from outlier vent sites (e.g. D or E1) have very few Oruanui eruption-age or older peak-age zircons (Figs 3 and 4). The potential for differences in source vertically within the crust is also considered unlikely as petrological studies suggest that the Oruanui and SG1 rhyolites were probably derived from similar shallow levels within the crust (~5–7 km; Sutton *et al.*, 1995; Smith *et al.*, 2005).

(2) All of the evolved melt-dominant body and mush zone was erupted in the Oruanui event, leaving little or no residual material behind with an associated zircon crystal suite. We also consider this unlikely given the large volume and crystal-poor nature of the Oruanui rhyolite and the likely volume of the counterpart magma mush root system (Wilson *et al.*, 2006; Allan *et al.*, 2013). Amphibole thermobarometry conducted on Oruanui low-Si (<74% SiO_2) and high-Si (>74% SiO_2) rhyolites suggests that the mush or source zone of the Oruanui magma system ranged between 6 and 12 km depth below a melt-dominant body at 3·5–6 km depth (Allan *et al.*, 2013). This huge magma system therefore probably covered the majority of the available vertical space in the quartzo-feldspathic crust below the Taupo area (Harrison & White, 2006) and leaves little room for crustal volumes not imprinted by Oruanui-related magmatic processes.

(3) The zircons extracted from the post-Oruanui samples are dominated by the growth of young zircons and any older population is effectively masked. This is not considered to be the dominant factor for three reasons. First, the post-Oruanui rhyolites have relatively low zircon yields (e.g. Charlier *et al.*, 2005) and are within a similar range of zircon saturation to the Oruanui magma (Watson, 1996; Boehnke *et al.*, 2013). Second, some units sampled have only a small proportion of young zircons (e.g. D and F), with populations dominated by older (equiline) grains, and even these units have few Oruanui-age zircons. Third, the largest post-Oruanui eruption studied (S) is roughly two orders of magnitude smaller than the Oruanui. Although the post-Oruanui magmas could be derived from localized magma pockets with correspondingly localized zircon growth, we suggest that the range of vent sites, repeated patterns of age spectra between eruptions and similar bulk-rock geochemistries (Sutton *et al.*, 2000) indicate a widespread change in the magma system.

(4) The majority of the Oruanui and pre-Oruanui age zircons were effectively removed from the crustal root zone by thermally induced dissolution in the aftermath of the Oruanui eruption and/or during the gestation process for each of the subsequent dacite to rhyolite magma batches. This cause is considered by us to be the most plausible.

Two lineages of mafic magmas played an important role in the Oruanui eruption (Wilson *et al.*, 2006), and they are likely to have had a strong thermal influence on the syn- or post-Oruanui magma system. The post-Oruanui dacites yield significantly higher magma temperature estimates (~920–940°C: Sutton *et al.*, 2000; Gelman *et al.*, 2013) than the younger rhyolites and also display evidence for some crustal melting through strongly resorbed plagioclase (Gelman *et al.*, 2013; S. J. Barker, unpublished data) and sparse unresorbed zircons from greywacke and Quaternary plutonic material (Charlier *et al.*, 2010). All of the post-Oruanui magmas have $^{87}Sr/^{86}Sr$ ratios elevated over those in the Oruanui eruption products (Sutton *et al.*, 2000; Wilson & Charlier, 2009; Fig. 2), which could reflect significant assimilation of crustal components immediately after the Oruanui eruption. Thermal calculations (Charlier *et al.*, 2010) indicate that zircons incorporated into strongly zircon-undersaturated, hot basaltic-andesite or dacite would be stable for only a few months to years (depending on their size fraction and surface area; Watson, 1996). If the whole Oruanui magma system underwent widespread post-eruption heating from mafic magma then the majority of the residual zircons left could have been dissolved. A minor fraction of either Oruanui and/or pre-Oruanui aged zircons, however, are still present in most samples [as previously documented by Charlier *et al.* (2005)]. The majority of Oruanui-age determinations are from resorbed zircon cores or interior zones (see Fig. 7 or Supplementary Data: Electronic Appendix B and C for the raw data), and hence represent the few zircons that partially survived thermal dissolution. The great majority of the pre-Oruanui zircons are either of Whakamaru age (300–500 ka; Fig. 6) for the northern-sourced magmas (Unit D, this study; Unit Ω, Charlier *et al.*, 2010) and therefore plutonic remnants, or pre-100 Ma in age (Unit F) and thus derived from the greywacke basement (Cawood *et al.*, 1999; Adams *et al.*, 2009; Charlier *et al.*, 2010). These xenocrystic zircons were probably incorporated into the post-Oruanui magmas through

partial assimilation or melting of local country rock, and are not necessarily therefore directly related to the Oruanui magmas.

Determining the nature and timing of post-supereruption zircon growth

Two dominant analytical techniques have proven to be invaluable for dating young zircons (and other accessory minerals where applicable; e.g. apatite, allanite) in igneous rocks. First, multiple crystals can be analysed by TIMS to give a highly precise mean age of the crystal population as a whole, with uncertainties typically of ~0·5–1·5 ka (2SD) for the young Taupo eruption units (Charlier *et al.*, 2005). Second, discrete domains within single crystals can be analysed by SIMS to give spatially resolved information, albeit at poorer precision. The TIMS data give a highly precise mean age, but must be treated with caution as the bulk zircon separate may represent multiple populations of diverse sources and age with no direct way of discriminating between them during preparation. As shown by Charlier *et al.* (2005), average TIMS model ages for post-Oruanui eruptions are in some cases <25·4 ka (e.g. Units B and E; Fig. 4), but also vary largely depending on size fractions (with smaller fractions usually being younger). In other cases (e.g. Units D, G and S) average bulk zircon ages are older and can be interpreted (based on our data here) as mixtures of xenocrysts from plutonic or greywacke source(s) with younger magmatic grains (Figs 4 and 5). In such cases, the diversity (or lack thereof) of average ages can be used as a good first-order approximation to interpret the likely variations in the makeup of zircon ages for any given sample. On the other hand, SIMS techniques yield single model ages, allowing for the identification of zircons that are probably phenocrystic versus those that were inherited from precursor magma systems (antecrystic) or from totally foreign magmas or country rocks (xenocrystic). SIMS analyses from our work give uncertainties that are at best ±2–3 ka (1SD) for young post-Oruanui grains but more commonly around ±4–8 ka (Supplementary Data: Electronic Appendix C). In such a case, differentiating between eruptions or magmatic events (periods of zircon growth or dissolution) that are spaced within, or close to the analytical uncertainty of a single model-age date can become difficult. Below we take into account the statistical significance of the analytical uncertainties to decide whether the clustering of model ages seen in the post-Oruanui SIMS datasets is real or is an artefact of the methods employed. Coupled with this analysis, we consider whether the similarities in clustering of model ages from successive units indicate that our measurements are accurate, despite the large uncertainties inherent in the analytical techniques.

Significance of age peaks identified in the post-Oruanui SIMS U–Th data

The dominance of zircons with model ages <25 ka in the post-Oruanui eruptions indicates that the majority of grains are inherent to the modern magma system. Two important questions arise from this observation, as follows.

(1) Over what time period following the Oruanui eruption did the Taupo rhyolite system rebuild and zircon growth recommence?
(2) Has the new magmatic system been in a steady state of recovery and/or evolution over time, and is it uniform over the geographical footprint of Taupo volcano?

Using the common approach of plotting zircon age data in probability density histograms (using Isoplot; Ludwig, 2008), several key features are apparent (Figs 3–5). The zircon model-age spectra from eruptions from both the SG1 and SG2 rhyolites show multiple peaks in binned histograms, suggesting that zircon growth has not occurred evenly through time. For the SG1 rhyolites, there appears to be a consistent peak close to the eruption age, with either a tail-off to older zircons or a secondary peak between slope 0·14 and 0·20. This bimodality is exemplified when all the SG1 age data are compiled into a single histogram (Fig. 8). However, binned histograms do not take into account the variable uncertainties of the single age determinations, bringing into question their statistical relevance in this study. Histogram bins have been chosen based on the lowest observed uncertainties (± slope 0·02) in an attempt to see small-scale variations in age spectra, but uncertainties on single data points can, in some cases, cover 3–4 bin spacings (Supplementary Data: Electronic Appendix C). The multiple histogram age peaks are largely lost, however, in the relative probability curve, which takes into account the different age uncertainties of all the single data points and effectively smooths out the histogram on the basis that the uncertainties do not permit the model-age data to be statistically distinguished from one population. For example, in several histograms the probability function curve is at a maximum between two modes in the histogram bars (e.g. Unit B1, Fig. 4d), because the chosen width of the histogram bins (i.e. slope 0·02) is within analytical uncertainty of some of the single (low-precision) data points. Similar issues occur with the SG2 rhyolites, which typically have an additional population of younger zircons and even more complicated age spectra, with some displaying two or three minor modes in histogram bins (Fig. 5). This problem of low (but variable) precision is further exemplified when the data are plotted on commonly used ($^{230}Th/^{232}Th$) vs ($^{238}U/^{232}Th$) equiline diagrams (Figs 3–5). Although equiline plots are useful for observing the overall range in isotopic systematics (which can then be converted to zircon model ages) and also variable analytical uncertainties, any closely spaced

clusters are drowned out by analyses with large uncertainties. Using these approaches, it is unclear whether the age peaks observed (and repeated) between eruptions are in fact real, and therefore represent multiple zircon populations, or are merely coincidental.

To address this we use Gaussian mixture modelling, which is commonly used to detect multiple components in the U–Pb age spectra of ancient detrital zircons and magmatic rocks (Sambridge & Compston, 1994; Jasra *et al.*, 2006). Mixture modelling allows for consideration of the variable uncertainties for single data points, and uses the maximum likelihood approach to estimate best fit for a suite of ages. It is particularly useful for identifying closely spaced age populations that cannot be easily quantitatively defined within the analytical uncertainties of the method used. Here we use a similar approach to that of Sambridge & Compston (1994), to determine whether the post-Oruanui zircon U–Th model-age spectra represent a single population within an acceptable spread, or multiple discrete populations (see Supplementary Data: Electronic Appendix F for further details). Because of the large number of U–Th analyses and apparent minor differences in age spectra over time, we calculated mixture models for the SG1 rhyolites and SG2 rhyolites separately, as well as a combination of the two datasets. Results are presented as contoured log-likelihoods with a 95% confidence interval (CI) and maximum log-likelihood representing the best fit point of the model, and additionally as cumulative probability curves to show the fit of the mixture model compared with the actual data and overall mean (Fig. 9).

For the SG1 rhyolites, a two-component mixture model gives a very good overall fit to the observed age data (Fig. 9a; Supplementary Data: Electronic Appendix F). The young population [slope (1)] is well defined with a maximum log-likelihood fit at slope 0·12 (equivalent to an age of ~14 ka) and a relatively narrow 95% CI of ~0·10–0·13 (~11·5–15 ka). As the majority of the data points in this model are included in the first slope, the second slope [slope (2)] is less well constrained and shows a broader 95% CI of slope between ~0·14 and 0·225, with a maximum log-likelihood ~0·186 (22·5 ka). The second population is affected by the large uncertainties on many of the zircons with model ages around ~20 ka with low U concentrations (Fig. 7; Supplementary Data: Electronic Appendix C).

For the SG2 rhyolites, the mixture model gives a good fit for a younger population, with a maximum log-likelihood for slope (1) at 0·086 (9·8 ka), but with a very poorly defined slope (2) owing to the low number of analyses included in this population (see Supplementary Data: Electronic Appendix F for details). The SG2 U–Th age spectra (Fig. 8) contain two young age peaks (0·06–0·08 and 0·10–0·12) in addition to an older ~0·16–0·18 slope peak, and a lower tail that stretches to younger ages than observed in the SG1 age spectra. However, the number of analyses in the SG2 sample set is insufficient for the data to be modelled using a three-component mixture model. Increasing the number of zircons in the populations by combining the two datasets (SG1 +SG2) produces a similar two-component result to that observed in the SG1 model, with maximum log-likelihood for slope (1) at 0·11 (12·7 ka) and that for slope (2) at 0·196 (23·8 ka) (Fig. 9b). In both the SG1 and SG2 datasets, the data can be modelled effectively using a two-component mixture with a well-defined young population that is represented by 85–90% of the data, and a minor but poorly defined older population. Mixture modelling therefore strongly supports the broad trends observed in the age histograms, and suggests that the multiple peaks observed in the model-age spectra are statistically significant, and reflect discrete zircon populations.

Controls on the timing of zircon growth in the post-Oruanui magmas

Zirconium saturation in magma and subsequent zircon growth is largely dependent on magma temperature (T_{magma}), the Zr content of the melt and the cation ratio M, where $M = (Na + K + 2Ca)/(Al \times Si)$ (Watson & Harrison, 1983; Watson, 1996; Boehnke *et al.*, 2013). T_{zirc} is defined as the magma temperature below which zirconium saturation is reached and zircon crystallization commences [although see Harrison *et al.* (2007)]. As shown by Charlier *et al.* (2005), magmas from Taupo span three scenarios of zircon growth or dissolution with variable magma temperature and composition, which we consider to be central to interpreting the trends seen in the zircon age spectra. In the first scenario, $T_{magma} < T_{zirc}$ where zirconium saturation in the magma is reached and zircon growth commences. The Oruanui high-Si rhyolite magma is an example of this scenario, with calculated Fe–Ti oxide temperatures of ~760–790°C closely coinciding with or slightly lower than the calculated T_{zirc} using the model of Watson & Harrison (1983) (Fig. 10). In the second scenario, $T_{magma} > T_{zirc}$ where the magma is above the temperature necessary for zirconium saturation and zircon dissolves, at a rate depending on the difference in temperature and the size of the zircon (Watson, 1996; Charlier *et al.*, 2010). The post-Oruanui dacites (Units Ψ, Ω and A) are examples of this scenario (Charlier *et al.*, 2005, 2010). The third scenario falls between the first two, where $T_{magma} \sim T_{zirc}$ and zircon does not grow or dissolve rapidly. The post-Oruanui rhyolites studied here lie between the first and third scenarios described above, with calculated T_{magma} either slightly higher than or similar to T_{zirc} within uncertainty of the Fe–Ti oxide thermometers (Fig. 10). In such a case, small fluctuations in temperature (20–30°C) over time may result in periods of crystallization of zircon during periods of magma cooling, or slight dissolution during periods of heating.

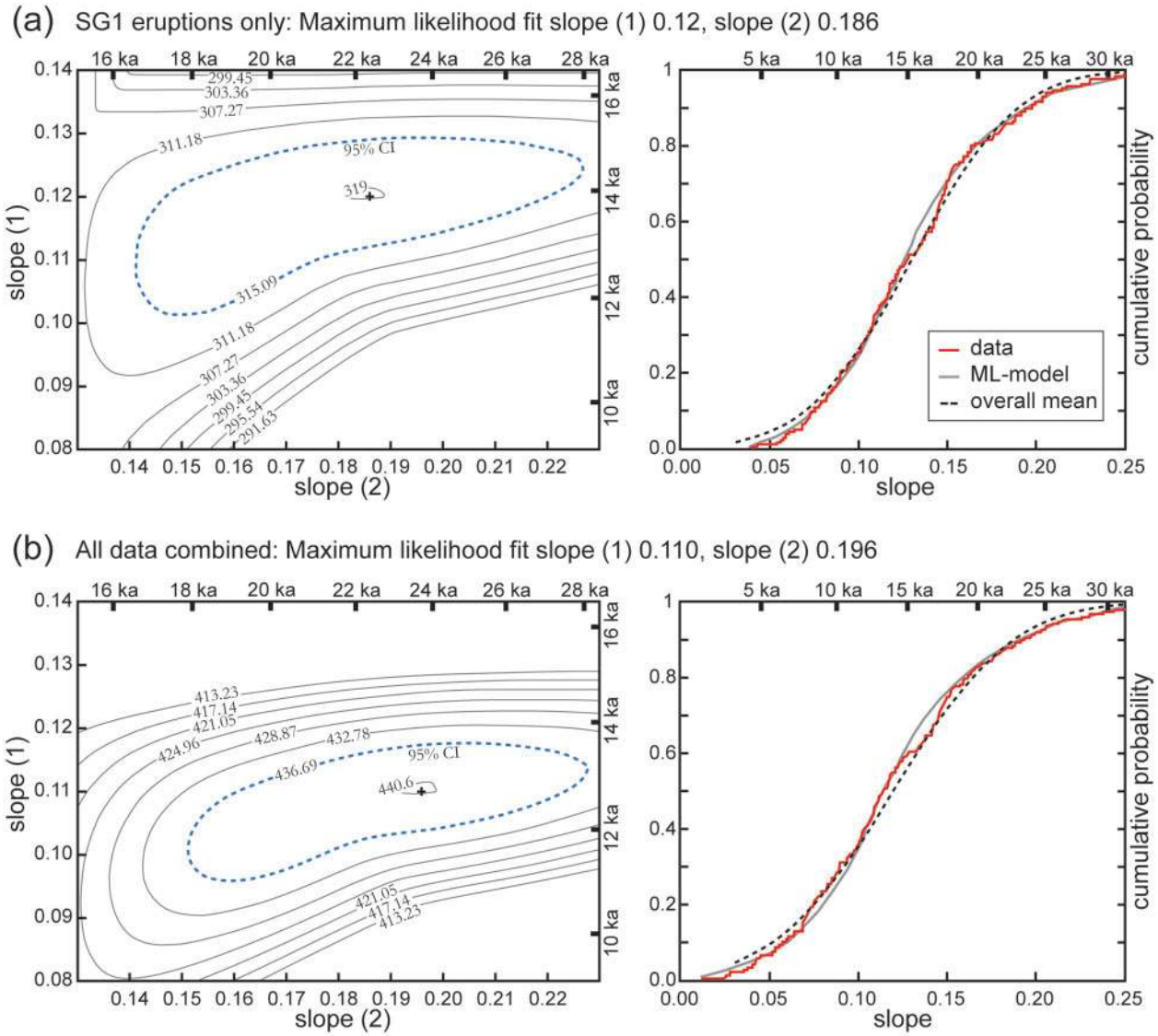

Fig. 9. Results of Gaussian mixture models for (a) the SG1 rhyolites (Units B, C, D and E) and (b) the SG1 and SG2 datasets combined. Contours represent log-likelihoods and the dashed contour represents a 95% confidence region for the two free parameters slope (1) and slope (2), conditional on the third factor alpha. Maximum log-likelihoods represent the best fit for the two-component mixture model. Calculated model ages are plotted opposite slope (2) for reference. (See Supplementary Data: Electronic Appendix F for model details and alpha value plots.)

The variability of zircon stability and growth in the post-Oruanui rhyolites is highlighted by several key features. First, there is a change in zircon abundance with eruption age, despite similar calculated magma temperatures for the various eruptive units, with zircon yields between the SG1 and SG2 rhyolites decreasing by an order of magnitude (Units B and E: $\sim$1·2 mg kg^{-1}; Unit G: 0·2 mg kg^{-1}; Unit S: 0·03 mg kg^{-1}; Charlier *et al.*, 2005). In addition, zircon morphology differs between the subgroups, being dominantly euhedral in the SG1 rhyolites to subhedral or anhedral in the SG2 rhyolites, suggesting that there is an accompanying reduction in relative zircon stability (Supplementary Data: Electronic Appendix B). Second, even with the presence of young zircons in the SG2 rhyolites, reflecting periods of crystallization, their age spectra are not wholly controlled by new zircon growth, but instead reflect a mixture with older inherited zircons (Fig. 8). Third, small increases in magma temperature in the youngest eruptive units at Taupo, which make up Subgroup 3 rhyolites (Units X, Y and Z; Sutton *et al.*, 2000; Fig. 10), have probably resulted in zircon dissolution (or non-growth) and subsequently the very low yields reported (Charlier *et al.*, 2005).

The observed age spectra in the post-Oruanui rhyolites clearly reflect a changing magma system with fluctuating magma temperatures, resulting in an overall reduction in

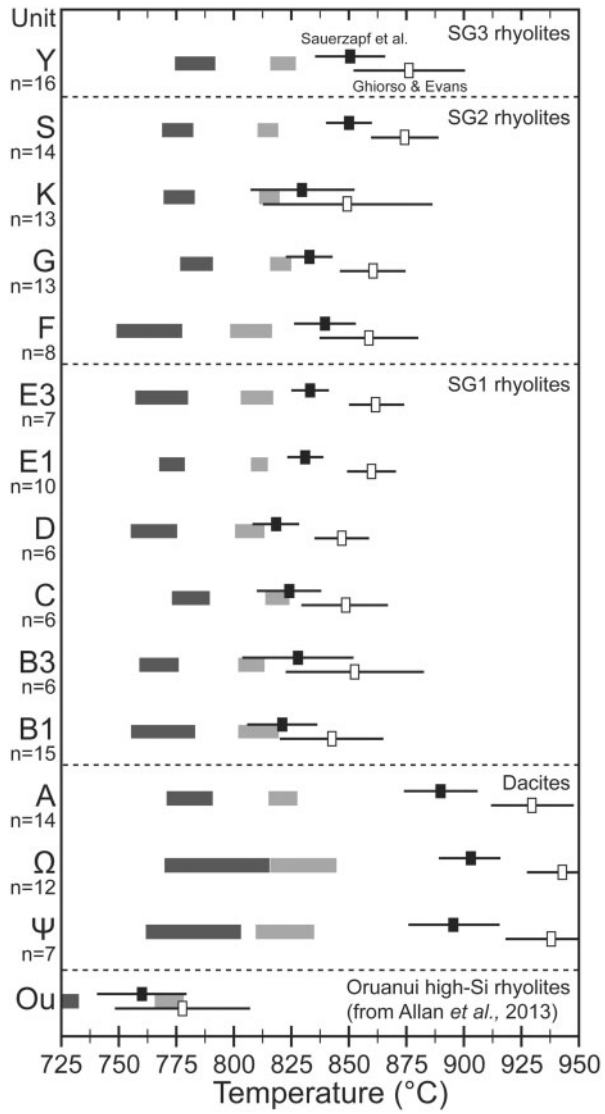

Fig. 10. Stacked Fe–Ti oxide model-temperature estimates and two zircon saturation temperature estimates (shaded rectangles). The zircon thermometer (light shading) uses the equations of Watson & Harrison (1983) whereas the dark shaded blocks use the equations of Boehnke *et al.* (2013) where the parameter $M = (\mathrm{Na} + \mathrm{K} + 2\mathrm{Ca})/(\mathrm{Al} \times \mathrm{Si})$. The zircon temperature range is from the range of M values calculated from multiple glass compositions determined on each eruptive unit by electron microprobe analysis (EPMA) at Victoria University of Wellington. The Fe–Ti oxide temperatures were calculated using the models of Ghiorso & Evans (2008) (open symbols) and Sauerzapf *et al.* (2008) (filled symbols), where the symbols are the average temperature and the lines on either side are 2SD. n is the number of Fe–Ti oxide pairs, also analysed by EPMA using similar methods to those of Barker *et al.* (2013). Oxide temperatures and glass compositions for the Oruanui eruption are from Allan *et al.* (2013), after Wilson *et al.* (2006).

zircon stability and growth through time. However, large or stepwise Fe–Ti oxide model temperature changes are not recorded between eruptions, either within or between the SG1 and SG2 rhyolite groups (Fig. 10), making the trends in zircon ages and abundance difficult to explain based on the volcanic record alone. Owing to their relatively fast diffusion rates, Fe–Ti oxides will provide only a snapshot of the magma immediately prior to quenching on eruption, and will not therefore reflect fluctuations in temperature and hence zircon growth between eruptions or eruptive subgroups. Using the Ti-in-zircon thermometer of Ferry & Watson (2007) it is apparent that there is a gradual increase in zircon model crystallization temperatures over time (Fig. 11a). This trend is in good agreement with observations of zircon abundance and textures in the post-Oruanui rhyolites, and probably reflects longer-term temperature changes in the magmatic system as Ti diffusion in zircon is extremely slow at these temperatures (Cherniak, 2010). Notably, the model temperatures of the Ferry & Watson (2007) thermometer are considerably lower than the average Fe–Ti oxide temperatures, although absolute temperatures using the Ti-in-zircon thermometer are dependent on the position in the crystal and the chosen method of estimating a value of $a\mathrm{TiO_2}$, and are variable by several tens of degrees centigrade with these factors (Ferry & Watson, 2007; Chamberlain *et al.*, 2014; Fig. 11a).

Determining the exact timing of periods of cooling and zircon crystallization is difficult because of the limitations of the model-age determinations. However, given the trends in the age spectra, Fe–Ti oxide and Ti-in-zircon temperatures, and the results of the mixture modelling, we consider that there are distinct periods of cooling and hence enhanced zircon crystallization in Taupo's magmatic system. The periods of enhanced crystallization appear to coincide with periods of volcanic quiescence. One dominant age population is defined in the SG1 ages as probably occurring between ~11·5 and ~15 ka, after the early dacites and just before eruption of the first rhyolites. In the SG2 rhyolites, this young population is supplemented by an additional population of zircons that probably formed post-10 ka but cannot be statistically resolved within age uncertainties. An older age population is present that is less well defined but coincides with the immediate post-Oruanui period during which eruption of the dacites from the northern part of Lake Taupo occurred from ~17 to 21 ka (Fig. 1). During this period, there was no known volcanism in the southern part of Lake Taupo, from which area the majority of the post-Oruanui rhyolites were vented. Although the dacite magmas were above zirconium saturation (as further supported by the scarcity of zircons in Unit D, also sourced from this area), part of the magma system to the south may have been cooling sufficiently to explain the older age peak observed in the SG1 and SG2 magmas. Opposing periods of cooling and crystallization at Taupo would be periods of magma rejuvenation and subsequent heating of the magma system. Hot mafic magmas are often closely linked with rhyolitic

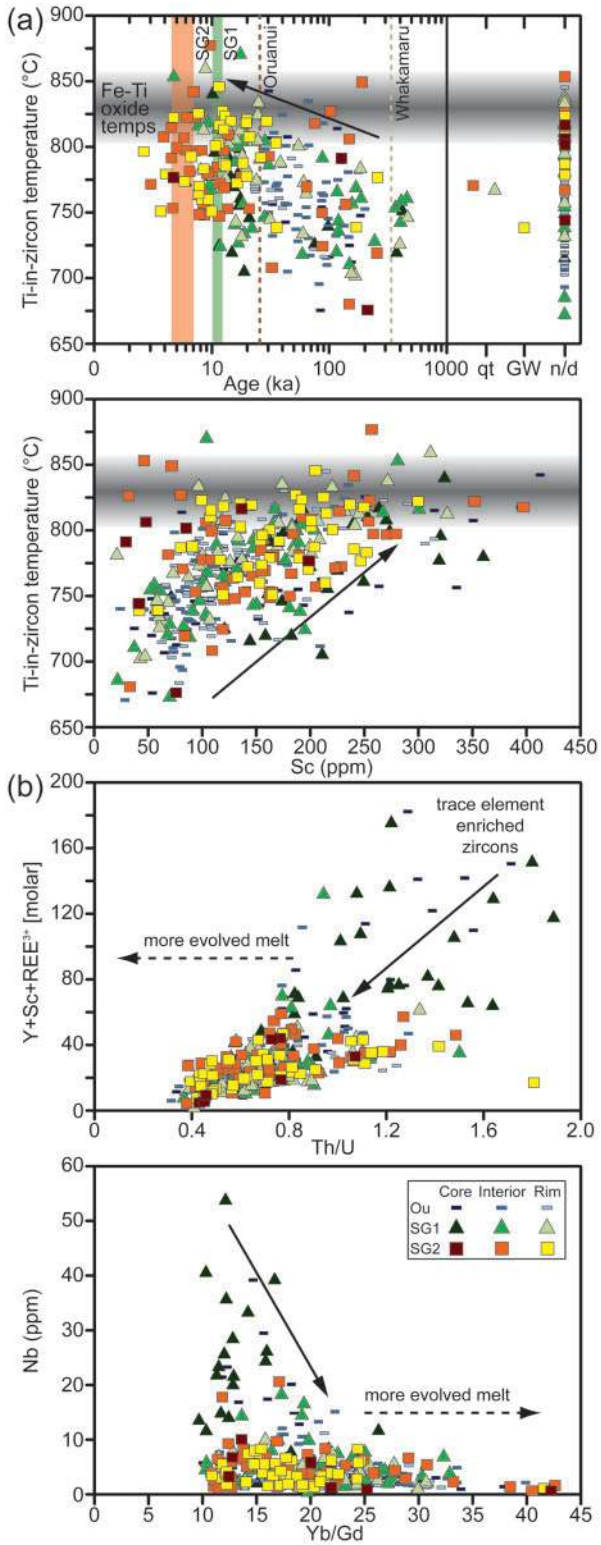

Fig. 11. Trace element and temperature variations in the Oruanui and post-Oruanui zircon populations. (a) Plots showing positive correlations between temperature estimates versus zircon age and Sc concentration using the Ti-in-zircon temperature model of Ferry & Watson (2007). $aTiO_2$ values for the Ti-in-zircon thermometer and magma temperatures were calculated using the Fe–Ti oxide model of Ghiorso & Evans (2008) and Sauerzapf *et al.* (2008) for each eruptive unit (Fe–Ti oxide temperature range for the post-Oruanui eruptions is shown by the dark shaded region). $aTiO_2$ typically varies between 0·50 and 0·55, being slightly higher in the Oruanui magma. Fe–Ti oxide compositions for the Oruanui are from Wilson *et al.* (2006). (b) Zircon trace element variations with differing degrees of inferred melt evolution. It should be noted that the zircons that crystallized from the least evolved melts have anomalously high concentrations of $Y + Sc + (REE)^{3+}$ and Nb. (See text for details.)

volcanism at Taupo (e.g. Blake *et al.*, 1992; Wilson *et al.*, 2006) and the broader TVZ (Leonard *et al.*, 2002; Hiess *et al.*, 2007; Rowland *et al.*, 2010). There is, in particular, evidence from the andesite cones south of Taupo that vigorous explosive activity there accompanied rifting and temporally bracketed the onset of SG1 rhyolitic volcanism at Taupo (Kohn & Topping, 1978; Nairn *et al.*, 1998). We suggest that a longer-term periodicity of magma-assisted rifting processes and higher rates of influx of mafic magmas into the crust below Taupo are the cause of the 5–10 kyr periodicity that is seen in the zircon crystallization history (during cooling and volcanic quiescence) and the clustering of eruptions into the subgroups (during rifting and volcanic activity).

Zircon compositions as tracers of changing melt compositions

In this study we have complemented zircon age determinations with trace element analyses of the same or similar growth zones within the same crystals. Minor and trace elements in zircon have proven particularly useful as they provide valuable insights into the composition of the magma from which they formed (Luo & Ayers, 2009; Barth *et al.*, 2013). In addition, the very low diffusivities of most elements in zircon allow zonation and independent phases of growth to be preserved over long timescales at the observed magmatic temperatures (Cherniak, 2010). Magmatic zircon typically incorporates minor and trace amounts of lithophile elements such as Sc, Y, REE, Ti, Hf, Th, U, Nb, Ta, V and P, which substitute for Zr and/or Si by either simple or coupled substitution mechanisms [for review see Hoskin & Schaltegger (2003)]. Elemental concentrations or ratios are used here to infer differing melt compositions between and within the Oruanui and post-Oruanui magma systems.

Two notable features of the combined trace element and age data provide evidence for distinct temporal variations in melt composition and conditions of crystallization, as follows.

(1) There is an overall increase in the Sc concentration with decreasing age between the Oruanui and post-Oruanui sourced zircons (Fig. 7). We attribute these trends to differences in the ferromagnesian crystal

phases that were stable in the melt at the time of zircon crystallization. Amphibole is the most likely phase found in the Taupo eruptive rocks that would change the concentration of Sc in the melt and hence zircon. Amphibole is present in Oruanui pumice, contributing up to ~5% of the crystal assemblage (Wilson *et al.*, 2006), but is relatively uncommon in the post-Oruanui eruptive rocks (Sutton *et al.*, 2000). In this study, amphibole was found as a minor phase in Units B and C (<2–3% of the crystal assemblage), at trace levels in Units D and E, and was absent in all the SG2 rhyolites. As Sc is ~20–40 times more enriched in the Oruanui amphiboles than the melt (Allan *et al.*, 2013), dissolution of amphibole would liberate Sc into the melt and make it available for substitution during zircon growth. As amphibole stability is largely dependent on temperature and the water content of the melt (Ridolfi *et al.*, 2010; Allan *et al.*, 2013), the observed gradual heating trend with time may explain the disappearance of amphibole in the younger units and the associated increase in Sc concentration in contemporaneously crystallizing zircons. In addition, Sc-rich zircons may reflect melts that have experienced recent magmatic rejuvenation. Sc concentrations are 3–4 times higher in the Oruanui mafic compositions than those observed in the rhyolites (Wilson *et al.*, 2006). Sc is broadly positively correlated with Ti-in-zircon model temperature, suggesting that the outlier high-Sc Oruanui zircon cores crystallized from hotter and possibly less evolved magmas (Fig. 11a).

(2) A small subpopulation of zircon core or interior analyses from the SG1 zircons and a few outlier grains from the Oruanui have anomalously high concentrations of U, Th, P, Y, $(REE)^{3+}$ and Nb (Fig. 7). U^{4+} and Th^{4+} substitute in zircon by simple substitution with Zr^{4+}, whereas (Y, $REE)^{3+}$ and P^{5+} dominantly substitute via xenotime substitution with Zr^{4+} + Si^{4+}, and Nb^{5+} couples with (Y, $REE)^{3+}$ for $2Zr^{4+}$ (Hoskin & Schaltegger, 2003). The range of experimentally calculated partition coefficients for these elements in zircon cannot explain the wide compositional variations observed in the Taupo zircons (Sano *et al.*, 2002). Sector zoned zircons in the Bishop Tuff have been recorded to show large differences in trace element concentrations (up to three times) between tips and sides in the same growth zone, suggesting that contrasting substitution mechanisms can occur within single crystals dependent on position on the crystal surface (Chamberlain *et al.*, 2014). However, sector zoning is relatively uncommon in zircons at Taupo, and the zircons do not display parallel arrays in the concentration of trace elements such as Ti, as is observed in the Bishop Tuff (see Supplementary Data: Electronic Appendix E). Instead, such high concentrations imply a substantial, but temporally (and spatially?) limited, change in melt composition. It should be noted that the post-Oruanui zircons with anomalously high trace element concentrations are limited to a subpopulation of SG1 zircon cores with model ages that range between 10 and 20 ka (Fig. 7; Supplementary Data: Electronic Appendices B and E). As previously discussed, there are several key lines of evidence that the Taupo magma system probably experienced large thermal changes owing to the influx of hot magma immediately after the Oruanui event. Dissolution of zircon, or potentially other U-, Th-, P-, Y- and $(REE)^{3+}$-bearing minerals such as apatite (Sano *et al.*, 2002), could then result in temporary but significant changes in melt composition. The first zircons to grow once the system reached zircon saturation (or the first zircons to grow in proximity to an area of partial melting), would then have enhanced levels of these elements. It is apparent that the zircons that grew during this period crystallized from the least evolved melts (i.e. highest Th/U ratio and lowest Yb/Gd ratio; Belousova *et al.*, 2002; Barth & Wooden, 2010) and have the highest concentration of U, Th, P, Y and $(REE)^{3+}$, but not necessarily Sc (Fig. 11b). Together with the U–Th zircon age spectra these observations imply that post-Oruanui heating of Taupo's magmatic system affected both the stability and composition of the zircons. Although the Oruanui zircons with cores or interior zones with anomalously high concentrations of U, Th, P, Y and $(REE)^{3+}$ do not cluster around any particular age interval (Fig. 7), we infer that these zircons partly grew in less evolved portions of the Oruanui magma system that had experienced earlier thermal fluxes and possible dissolution prior to eruption. Less evolved melts, such as the low-Si rhyolite described by Allan *et al.* (2013), may be the source of such enrichments.

CONCLUSIONS

Zircon U–Th and U–Pb ages along with complementary trace element data yield insights into how the magmatic system at Taupo was rapidly destroyed then rebuilt after the 25·4 ka Oruanui supereruption. U–Th zircon model ages for the first erupted SG1 rhyolites at 12 ka mostly post-date the Oruanui eruption, indicating limited inheritance of crystals from the two dominant model-age modes (40 and 95 ka) in the Oruanui magma source. Subsequent eruptive units from multiple vents also contain only sparse numbers of Oruanui-age or Oruanui peak-age grains and are instead consistently dominated by multiple young peaks in their model-age spectra. Two lava-dominated eruptions (D and F) from vents at the northern and

southern limits of the young vent sites respectively contain a high proportion of old U–Th equiline zircons. When dated by U–Pb techniques these old grains are a mixture of 300–450 ka plutonic-derived and pre-100 Ma greywacke basement-derived grains. Plutonic-derived grains mostly match in age published zircon age determinations from the Whakamaru eruption (Brown & Fletcher, 1999; 350 ka), and are dominant in young units from the northern part of Taupo that overlap with the proposed Whakamaru caldera outline. The scarcity of grains in the post-Oruanui units with ages that match the Oruanui or its modes is interpreted to have been caused by thermal dissolution in the immediate post-supereruption magma system, induced by instabilities resulting from the evacuation of a huge magma body and large influxes of hot mafic magma. This concept is supported by the trace element data, which show a subpopulation of post-Oruanui zircons enriched in U, Th, P, Y and $(REE)^{3+}$, representing crystals that grew following dissolution in the post-supereruption magma system. There is also a pronounced rise in the Sr isotopic values recorded between the Oruanui magma compositions and the post-Oruanui eruptive rocks (whether dacitic or rhyolitic) (Sutton *et al.*, 2000; Wilson & Charlier, 2009). This increase implies that the changes in the immediate aftermath of the Oruanui eruption also involved influx of a more radiogenic source component, most logically basement greywacke. Longer-term trends in zircon trace element chemistry, such as increasing Sc concentrations, reflect changing amphibole stability in the source region as the system generated progressively hotter magmas with time.

The magma system at Taupo was effectively reset following the Oruanui event, with little or no magmatic record of the preceding supersized magma system. Finer detail within the young zircon U–Th age spectra reveals the consistent inheritance of young post-Oruanui grains between the temporally spaced but geographically overlapping eruption groups. Using Gaussian mixture modelling, we interpret repeated peaks within the age spectra to be statistically significant and to result from recycling of crystals from multiple age populations. Taupo's rhyolitic system rapidly rebuilt following the Oruanui eruption, but not smoothly over time. Zircon stability in Taupo's young magma system was variable and crystallization (and hence melt evolution) probably occurred in episodic cooling cycles, reflecting periods of volcanic quiescence and crystallization. The modern rhyolitic subgroups are closely related, and record a system that has gradually heated over time. In conjunction with other studies on zircon age spectra at Taupo (Charlier *et al.*, 2005; Wilson & Charlier, 2009), we conclude that supervolcanic systems can operate on geologically rapid timescales. In the case study of Taupo, a supersized magma system was constructed over tens of millennia, finally assembled in centuries to millennia, and effectively destroyed, and then a new magmatic system was rebuilt on equally rapid timescales.

ACKNOWLEDGEMENTS

We thank Matt Coble, John Foster, Peter Holden and Brad Ito for their help and assistance in the SHRIMP laboratories at Stanford and ANU. We also thank Drew Coleman and an anonymous reviewer for their insightful suggestions, and Simon Turner for editorial handling.

FUNDING

We acknowledge financial support from the Marsden Fund of the Royal Society of New Zealand (Grant VUW0813), a Royal Society of New Zealand James Cook Fellowship to C.J.N.W., a Victoria University Doctoral Scholarship awarded to S.J.B. and two Victoria University Strategic Research Grants and a Postgraduate Research Excellence Award for S.J.B.

SUPPLEMENTARY DATA

Supplementary data for this paper are available at *Journal of Petrology* online.

REFERENCES

Adams, C. J., Mortimer, N., Campbell, H. J. & Griffin, W. J. (2009). Age/isotopic characterisation of Torlesse Supergroup and Waipapa Group metasediments in the central North Island, New Zealand. *New Zealand Journal of Geology and Geophysics* **52**, 149–170.

Allan, A. S. R., Wilson, C. J. N., Millet, M.-A. & Wysoczanski, R. J. (2012). The invisible hand: tectonic triggering and modulation of a rhyolitic supereruption. *Geology* **40**, 563–566.

Allan, A. S. R., Morgan, D. J., Wilson, C. J. N. & Millet, M.-A. (2013). From mush to eruption in centuries: assembly of the super-sized Oruanui magma body. *Contributions to Mineralogy and Petrology* **166**, 143–164.

Aramaki, S. (1984). Formation of the Aira Caldera, southern Kyushu, ~22,000 years ago. *Journal of Geophysical Research* **89**, 8485–8501.

Bachmann, O., Dungan, M. A. & Lipman, P. W. (2002). The Fish Canyon magma body, San Juan volcanic field, Colorado: rejuvenation and eruption of an upper crustal batholith. *Journal of Petrology* **43**, 1469–1503.

Barker, S. J., Wilson, C. J. N., Baker, J. A., Millet, M.-A., Rotella, M. D., Wright, I. C. & Wysoczanski, R. J. (2013). Geochemistry and petrogenesis of silicic magmas in the intra-oceanic Kermadec arc. *Journal of Petrology* **54**, 351–391.

Barth, A. P. & Wooden, J. L. (2010). Coupled elemental and isotopic analyses of polygenetic zircons from granitic rocks by ion microprobe, with implications for melt evolution and the sources of granitic magmas. *Chemical Geology* **277**, 149–159.

Barth, A. P., Wooden, J. L., Jacobson, C. E. & Economos, R. C. (2013). Detrital zircon as a proxy for tracking the magmatic arc system: The California arc example. *Geology* **41**, 223–226.

Belousova, E. A., Griffin, W. L., O'Reilly, S. Y. & Fisher, N. I. (2002). Igneous zircon: trace element composition as an indicator of source rock type. *Contributions to Mineralogy and Petrology* **143**, 602–622.

Bindeman, I. N., Valley, J. W., Wooden, J. L. & Persing, H. M. (2001). Post-caldera volcanism: *in situ* measurement of U–Pb age and oxygen isotope ratio in Pleistocene zircons from Yellowstone caldera. *Earth and Planetary Science Letters* **189**, 197–206.

Black, L. P., Kamo, S. L., Allen, C. M., Davis, D. W., Aleinikoff, J. N., Valley, J. W., Mundil, R.M., Campbell, I. H., Korsch, R. J., Williams, I. S. & Foudoulis, C. (2004). Improved $^{206}Pb/^{238}U$ microprobe geochronology by the monitoring of a trace-element-related matrix effect: SHRIMP, ID-TIMS, ELA-ICP-MS, and oxygen isotope documentation for a series of zircon standards. *Chemical Geology* **205**, 115–140.

Blake, S., Wilson, C. J. N., Smith, I. E. M. & Walker, G. P. L. (1992). Petrology and dynamics of the Waimihia mixed magma eruption, Taupo Volcano, New Zealand. *Journal of the Geological Society, London* **149**, 193–207.

Boehnke, P., Watson, E. B., Trail, D., Harrison, T. M. & Schmitt, A. K. (2013). Zircon saturation re-revisited. *Chemical Geology* **351**, 324–334.

Brown, S. J. A. & Fletcher, I. R. (1999). SHRIMP U–Pb dating of the pre-eruption growth history of zircons from the 340 ka Whakamaru Ignimbrite, New Zealand: Evidence for >250 k.y magma residence times. *Geology* **27**, 1035–1038.

Cawood, P. A., Nemchin, A. A., Leverenz, A., Saeed, A. & Ballance, P. F. (1999). U/Pb dating of detrital zircons: Implications for the provenance record of Gondwana margin terranes. *Geological Society of America Bulletin* **111**, 1107–1119.

Chamberlain, K. J., Wilson, C. J. N., Wooden, J. L., Charlier, B. L. A. & Ireland, T. R. (2014). New perspectives on the Bishop Tuff from zircon textures, ages and trace elements. *Journal of Petrology* **55**, 395–426.

Charlier, B. L. A. & Wilson, C. J. N. (2010). Chronology and evolution of caldera-forming and post-caldera magma systems at Okataina volcano, New Zealand from zircon U/Th model-age spectra. *Journal of Petrology* **51**, 1121–1141.

Charlier, B. L. A., Wilson, C. J. N., Lowenstern, J. B., Blake, S., van Calsteren, P. W. & Davidson, J. P. (2005). Magma generation at a large, hyperactive silicic volcano (Taupo, New Zealand) revealed by U–Th and U–Pb systematics in zircons. *Journal of Petrology* **46**, 3–32.

Charlier, B. L. A., Wilson, C. J. N. & Davidson, J. P. (2008). Rapid open-system assembly of a large silicic magma body: time-resolved evidence from cored plagioclase crystals in the Oruanui eruption deposits, New Zealand. *Contributions to Mineralogy and Petrology* **156**, 799–813.

Charlier, B. L. A., Wilson, C. J. N. & Mortimer, N. (2010). Evidence from zircon U–Pb age spectra for crustal structure and felsic magma genesis at Taupo volcano, New Zealand. *Geology* **38**, 915–918.

Cherniak, D. J. (2010). Diffusion in accessory minerals: zircon, titanite, apatite, monazite and xenotime. In: Zhang, Y. & Cherniak, D. J. (eds) *Diffusion in Minerals and Melts. Mineralogical Society of America and Geochemical Society, Reviews in Mineralogy and Geochemistry* **72**, 827–869.

Chesner, C. A. (2012). The Toba caldera complex. *Quaternary International* **258**, 5–18.

Ferry, J. M. & Watson, E. B. (2007). New thermodynamic models and revised calibrations for the Ti-in-zircon and Zr-in-rutile thermometers. *Contributions to Mineralogy and Petrology* **154**, 429–437.

Gelman, S. E., Deering, C. D., Gutierrez, F. J. & Bachmann, O. (2013). Evolution of the Taupo volcanic center, New Zealand: petrological and thermal constraints from the Omega dacite. *Contributions to Mineralogy and Petrology* **166**, 1355–1374.

Ghiorso, M. S. & Evans, B. W. (2008). Thermodynamics of rhombohedral oxide solid solutions and a revision of the Fe–Ti two-oxide geothermometer and oxygen barometer. *American Journal of Science* **308**, 957–1039.

Girard, G. & Stix, J. (2009). Buoyant replenishment in silicic magma reservoirs: Experimental approach and implications for magma dynamics, crystal mush remobilization, and eruption. *Journal of Geophysical Research* **114**, B08203.

Harrison, A. & White, R. S. (2006). Lithospheric structure of an active backarc basin: the Taupo Volcanic Zone, New Zealand. *Geophysical Journal International* **167**, 968–990.

Harrison, T. M., Watson, E. B. & Aikman, A. B. (2007). Temperature spectra of zircon crystallization in plutonic rocks. *Geology* **35**, 635–638.

Hiess, J., Cole, J. W. & Spinks, K. D. (2007). Influence of the crust and crustal structure on the location and composition of high-alumina basalts of the Taupo Volcanic Zone, New Zealand. *New Zealand Journal of Geology and Geophysics* **50**, 327–342.

Hildreth, W. (1981). Gradients in silicic magma chambers: implications for lithospheric magmatism. *Journal of Geophysical Research* **86**, 10153–10192.

Hildreth, W. (2004). Volcanological perspectives on Long Valley, Mammoth Mountain, and Mono Craters: several contiguous but discrete systems. *Journal of Volcanology and Geothermal Research* **136**, 169–198.

Hildreth, W. & Wilson, C. J. N. (2007). Compositional zoning of the Bishop Tuff. *Journal of Petrology* **48**, 951–999.

Hoskin, P. W. O. & Schaltegger, U. (2003). The composition of zircon and igneous and metamorphic petrogenesis. In: Hanchar, J. M. & Hoskin, P. W. O. (eds) *Zircon. Mineralogical Society of America and Geochemical Society, Reviews in Mineralogy and Geochemistry* **53**, 27–62.

Jasra, A., Stephens, D. A., Gallagher, K. & Holmes, C. C. (2006). Bayesian mixture modelling in geochronology via Markov chain Monte Carlo. *Mathematical Geology* **38**, 269–300.

Kohn, B. P. & Topping, W. W. (1978). Time–space relationships between late Quaternary rhyolitic and andesitic volcanism in the southern Taupo Volcanic Zone, New Zealand. *Geological Society of America Bulletin* **89**, 1265–1271.

Leonard, G. S. (2003). The evolution of Maroa Volcanic Centre, Taupo Volcanic Zone, New Zealand. Christchurch: PhD thesis, University of Canterbury.

Leonard, G. S., Cole, J. W., Nairn, I. A. & Self, S. (2002). Basalt triggering of the *c.* AD 1305 Kaharoa rhyolite eruption, Tarawera Volcanic Complex, New Zealand. *Journal of Volcanology and Geothermal Research* **115**, 461–486.

Leonard, G. S., Begg, J. G. & Wilson, C. J. N. (compilers) (2010). *Geology of the Rotorua area. Institute of Geological and Nuclear Sciences 1:250,000 geological map 5.* Lower Hutt: GNS Science.

Lindsay, J. M., Schmidt, A. K., Trumbull, R. B., de Silva, S. L., Siebel, W. & Emmermann, R. (2001). Magmatic evolution of the La Pacana Caldera system, Central Andes, Chile: compositional variation of two cogenetic, large-volume felsic ignimbrites. *Journal of Petrology* **42**, 459–486.

Liu, Y., Anderson, A. T., Wilson, C. J. N., Davis, A. M. & Steele, I. M. (2006). Mixing and differentiation in the Oruanui rhyolitic magma, Taupo, New Zealand: evidence from volatiles and trace elements in melt inclusions. *Contributions to Mineralogy and Petrology* **151**, 71–87.

Ludwig, K. R. (2008). *Isoplot/Ex version 3.70, A Geochronological Toolkit for Microsoft Excel. Berkeley Geochronology Center Special Publications* **4**.

Luo, Y. & Ayers, J. C. (2009). Experimental measurements of zircon/melt trace element partition coefficients. *Geochimica et Cosmochimica Acta* **73**, 3656–3679.

Mason, B. G., Pyle, D. M. & Oppenheimer, C. (2004). The size and frequency of the largest explosive eruptions on Earth. *Bulletin of Volcanology* **66**, 735–748.

Matthews, N. E. (2011). Magma chamber assembly and dynamics of a supervolcano: Whakamaru, Taupo Volcanic Zone, New Zealand. PhD thesis, University of Oxford.

Matthews, N. E., Pyle, D. M., Smith, V. C., Wilson, C. J. N., Huber, C. & van Hinsberg, V. (2012). Quartz zoning and the pre-eruptive evolution of the ~340-ka Whakamaru magma systems, New Zealand. *Contributions to Mineralogy and Petrology* **163**, 87–107.

McConnell, V. S., Shearer, C. K., Eichelberger, J. C., Keskinen, M. J., Layer, P. W. & Papike, J. J. (1995). Rhyolite intrusions in the intracaldera Bishop Tuff, Long Valley caldera, California. *Journal of Volcanology and Geothermal Research* **67**, 41–60.

Miller, C. F. & Wark, D. A. (2008). Supervolcanoes and their explosive supereruptions. *Elements* **4**, 11–16.

Nairn, I. A., Kobayashi, T. & Nakagawa, M. (1998). The ~10 ka multiple vent pyroclastic eruption sequence at Tongariro Volcanic Centre, Taupo Volcanic Zone, New Zealand: Part 1. Eruptive processes during regional extension. *Journal of Volcanology and Geothermal Research* **86**, 19–44.

Phillips, E. H., Goff, F., Kyle, P. R., McIntosh, W. C., Dunbar, N. W. & Gardner, J. N. (2007). The $^{40}Ar/^{39}Ar$ age constraints on the duration of resurgence at the Valles caldera, New Mexico. *Journal of Geophysical Research* **112**, B08201.

Reid, M. R. (2008). How long does it take to supersize an eruption? *Elements* **4**, 23–28.

Reid, M. R. & Coath, C. D. (2000). *In situ* U–Pb ages of zircons from the Bishop Tuff: No evidence for long crystal residence times. *Geology* **28**, 443–446.

Reid, M. R., Coath, C. D., Harrison, T. M. & McKeegan, K. D. (1997). Prolonged residence times for the youngest rhyolites associated with Long Valley caldera: $^{230}Th–^{238}U$ ion microprobe dating of young zircons. *Earth and Planetary Science Letters* **150**, 27–39.

Ridolfi, F., Renzulli, A. & Puerini, M. (2010). Stability and chemical equilibrium of amphibole in calc-alkaline magmas: an overview, new thermobarometric formulations and application to subduction-related volcanoes. *Contributions to Mineralogy and Petrology* **160**, 45–66.

Rowland, J. V., Wilson, C. J. N. & Gravley, D. M. (2010). Spatial and temporal variations in magma-assisted rifting, Taupo Volcanic Zone, New Zealand. *Journal of Volcanology and Geothermal Research* **190**, 89–108.

Sambridge, M. S. & Compston, W. (1994). Mixture modelling of multi-component data sets with application to ion-probe zircon ages. *Earth and Planetary Science Letters* **128**, 373–390.

Sano, Y., Terada, K. & Fukuoka, T. (2002). High mass resolution ion microprobe analysis of rare earth elements in silicate glass, apatite and zircon: lack of matrix dependency. *Chemical Geology* **184**, 217–230.

Sauerzapf, U., Lattard, D., Burchard, M. & Engelman, R. (2008). The titanomagnetite–ilmenite equilibrium: new experimental data and thermo-oxybarometric application to the crystallization of basic to intermediate rocks. *Journal of Petrology* **49**, 1161–1185.

Saunders, K. E., Baker, J. A. & Wysoczanski, R. J. (2010). Microanalysis of large volume silicic magma in continental and oceanic arcs: melt inclusions in Taupo Volcanic Zone and Kermadec Arc rocks, South West Pacific. *Journal of Volcanology and Geothermal Research* **190**, 203–218.

Schärer, U. (1984). The effect of initial ^{230}Th disequilibrium on young U–Pb ages: the Makalu case, Himalaya. *Earth and Planetary Science Letters* **67**, 191–204.

Schmitt, A. K., Stockli, D. F., Lindsay, J. M., Robertson, R., Lovera, O. M. & Kislitsyn, R. (2010). Episodic growth and homogenization of plutonic roots in arc volcanoes from combined U–Th and (U–Th)/He zircon dating. *Earth and Planetary Science Letters* **295**, 91–103.

Self, S. (2006). The effects and consequences of very large explosive volcanic eruptions. *Philosophical Transactions of the Royal Society of London, Series A* **364**, 2073–2097.

Simon, J. I. & Reid, M. R. (2005). The pace of rhyolite differentiation and storage in an 'archetypical' silicic magma system, Long Valley, California. *Earth and Planetary Science Letters* **235**, 123–140.

Simon, J. I., Renne, P. R. & Mundil, R. (2008). Implications of pre-eruptive magmatic histories of zircons for U–Pb geochronology of silicic extrusions. *Earth and Planetary Science Letters* **266**, 182–194.

Simon, J. I., Vazquez, J. A., Renne, P. R., Schmitt, A. K., Bacon, C. R. & Reid, M. R. (2009). Accessory mineral U–Th–Pb ages and $^{40}Ar/^{39}Ar$ eruption chronology, and their bearing on rhyolitic magma evolution in the Pleistocene Coso volcanic field, California. *Contributions to Mineralogy and Petrology* **158**, 421–446.

Smith, V. C., Shane, P. & Nairn, I. A. (2005). Trends in rhyolite geochemistry, mineralogy, and magma storage during the last 50 kyr at Okataina and Taupo volcanic centres, Taupo Volcanic Zone, New Zealand. *Journal of Volcanology and Geothermal Research* **148**, 372–406.

Stacey, J. S. & Kramers, J. D. (1975). Approximation of terrestrial lead isotope evolution by a two-stage model. *Earth and Planetary Science Letters* **26**, 207–221.

Stix, J., Goff, F., Gorton, M. P., Heiken, G. & Garcia, S. R. (1988). Restoration of compositional zonation in the Bandelier silicic magma chamber between two caldera-forming eruptions: geochemistry and origin of the Cerro Toledo Rhyolite, Jemez Mountains, New Mexico. *Journal of Geophysical Research* **93**, 6129–6147.

Storm, S., Shane, P., Schmitt, A. K. & Lindsay, J. M. (2011). Contrasting punctuated zircon growth in two syn-erupted rhyolite magmas from Tarawera volcano: Insights to crystal diversity in magmatic systems. *Earth and Planetary Science Letters* **301**, 511–520.

Sutton, A. N., Blake, S. & Wilson, C. J. N. (1995). An outline geochemistry of rhyolite eruptives from Taupo volcanic centre, New Zealand. *Journal of Volcanology and Geothermal Research* **68**, 153–175.

Sutton, A. N., Blake, S., Wilson, C. J. N. & Charlier, B. L. A. (2000). Late Quaternary evolution of a hyperactive rhyolite magmatic system: Taupo volcanic centre, New Zealand. *Journal of the Geological Society, London* **157**, 537–552.

Vandergoes, M. J., Hogg, A. G., Lowe, D. J., Newnham, R. M., Denton, G. H., Southon, J., Barrell, D. J. A., Wilson, C. J. N., McGlone, M. S., Allan, A. S. R., Almond, P. C., Petchey, F., Dabell, K., Dieffenbacher-Krall, A. C. & Blaauw, M. (2013). A revised age for the Kawakawa/Oruanui tephra, a key marker for the Last Glacial Maximum in New Zealand. *Quaternary Science Reviews* **74**, 195–201.

Van Eaton, A. R. & Wilson, C. J. N. (2013). The nature, origins and distribution of ash aggregates in a large-scale wet eruption deposit: Oruanui, New Zealand. *Journal of Volcanology and Geothermal Research* **250**, 129–154.

Vazquez, J. A. & Reid, M. R. (2002). Time scales of magma storage and differentiation of voluminous high-silica rhyolites at Yellowstone caldera, Wyoming. *Contributions to Mineralogy and Petrology* **144**, 274–285.

Vazquez, J. A. & Reid, M. R. (2004). Probing the accumulation history of the voluminous Toba magma. *Science* **305**, 991–994.

Vazquez, J. A., Kyriazis, S. F., Reid, M. R., Sehler, R. C. & Ramos, F. C. (2009). Thermochemical evolution of young rhyolites at Yellowstone: Evidence for a cooling but periodically replenished postcaldera magma reservoir. *Journal of Volcanology and Geothermal Research* **188**, 186–196.

Watson, E. B. (1996). Dissolution, growth and survival of zircons during crustal fusion: kinetic principles, geological models and implications for isotopic inheritance. *Transactions of the Royal Society of Edinburgh: Earth Sciences* **87**, 43–56.

Watson, E. B. & Harrison, T. M. (1983). Zircon saturation revisited: temperature and composition effects in a variety of crustal magma types. *Earth and Planetary Science Letters* **64**, 295–304.

Watts, K. E., Bindeman, I. N. & Schmitt, A. K. (2012). Crystal scale anatomy of a dying supervolcano: an isotope and geochronology study of individual phenocrysts from voluminous rhyolites of the Yellowstone caldera. *Contributions to Mineralogy and Petrology* **164**, 45–67.

Wilson, C. J. N. (1993). Stratigraphy, chronology, styles and dynamics of late Quaternary eruptions from Taupo volcano, New Zealand. *Philosophical Transactions of the Royal Society of London, Series A* **343**, 205–306.

Wilson, C. J. N. (2001). The 26·5 ka Oruanui eruption, New Zealand: an introduction and overview. *Journal of Volcanology and Geothermal Research* **112**, 133–174.

Wilson, C. J. N. & Charlier, B. L. A. (2009). Rapid rates of magma generation at contemporaneous magma systems, Taupo volcano, New Zealand: insights from U–Th model-age spectra in zircons. *Journal of Petrology* **50**, 875–907.

Wilson, C. J. N., Houghton, B. F. & Lloyd, E. F. (1986). Volcanic history and evolution of the Maroa–Taupo area, central North Island. In: Smith, I. E. M. (ed.) *Late Cenozoic Volcanism in New Zealand. Royal Society of New Zealand Bulletin* **23**, 194–223.

Wilson, C. J. N., Houghton, B. F., McWilliams, M. O., Lanphere, M. A., Weaver, S. D. & Briggs, R. M. (1995). Volcanic and structural evolution of Taupo Volcanic Zone, New Zealand: a review. *Journal of Volcanology and Geothermal Research* **68**, 1–28.

Wilson, C. J. N., Blake, S., Charlier, B. L. A. & Sutton, A. N. (2006). The 26·5 ka Oruanui eruption, Taupo volcano, New Zealand: development, characteristics and evacuation of a large rhyolitic magma body. *Journal of Petrology* **47**, 35–69.

Wilson, C. J. N., Gravley, D. M., Leonard, G. S. & Rowland, J. V. (2009). Volcanism in the central Taupo Volcanic Zone, New Zealand: tempo, styles and controls. In: Thordarson, T., Self, S., Larsen, G., Rowland, S. K. & Hoskuldsson, A. (eds) *Studies in Volcanology: The Legacy of George Walker. Special Publications of IAVCEI* **2**, 225–247.